

Geometric Aspects of Entanglement Generating Hamiltonian Evolutions

Carlo Cafaro¹ and James Schneeloch^{21,2}

¹¹University at Albany-SUNY, Albany, NY 12222, USA

²²Air Force Research Laboratory, Information Directorate, Rome, New York, 13441, USA

We examine the pertinent geometric characteristics of entanglement that arise from stationary Hamiltonian evolutions transitioning from separable to maximally entangled two-qubit quantum states. From a geometric perspective, each evolution is characterized by means of geodesic efficiency, speed efficiency, and curvature coefficient. Conversely, from the standpoint of entanglement, these evolutions are quantified using various metrics, such as concurrence, entanglement power, and entangling capability.

Overall, our findings indicate that time-optimal evolution trajectories are marked by high geodesic efficiency, with no energy resource wastage, no curvature (i.e., zero bending), and an average path entanglement that is less than that observed in time-suboptimal evolutions. Additionally, when analyzing separable-to-maximally entangled evolutions between nonorthogonal states, time-optimal evolutions demonstrate a greater short-time degree of nonlocality compared to time-suboptimal evolutions between the same initial and final states. Interestingly, the reverse is generally true for separable-to-maximally entangled evolutions involving orthogonal states. Our investigation suggests that this phenomenon arises because suboptimal trajectories between orthogonal states are characterized by longer path lengths with smaller curvature, which are traversed with a higher energy resource wastage compared to suboptimal trajectories between nonorthogonal states. Consequently, a higher initial degree of nonlocality in the unitary time propagators appears to be essential for achieving the maximally entangled state from a separable state. Furthermore, when assessing optimal and suboptimal evolutions from initial to final states while maintaining a constant degree of entanglement change, irrespective of whether they are orthogonal, the average speed of path entanglement is inversely related to the duration of travel and, additionally, directly related to the variation in concurrence. In summary, dynamic paths that exhibit greater (instantaneous) evolution speeds are also defined by higher (average) path entanglement speeds.

PACS numbers: Quantum Computation (03.67.Lx), Quantum Information (03.67.Ac), Quantum Mechanics (03.65.-w).

I. INTRODUCTION

The relationship between nonlocality and entanglement in quantum theory is nontrivial [1–4]. For instance, entangled states exhibit nonlocality as they violate Bell-type inequalities (known as Bell nonlocality [5–8]). Nevertheless, nonlocal characteristics are not exclusive to entangled systems. Specifically, one might anticipate that if the states of a quantum system were confined to a set of orthogonal product states, the system would function entirely in a classical manner and would not display any nonlocality. Moreover, it should be feasible to ascertain the state of the system using only local measurements. Surprisingly, this is not the case. In Ref. [2], Bennett and his colleagues devised sets of product states that cannot be precisely distinguished through local operations and classical communication (LOCC), even though their mutual orthogonality guarantees perfect global discrimination. The observation that nonlocal behavior in quantum theory does not always require entanglement also arises when examining quantum operations. Notably, while the SWAP operation transforms product states into product states, its nonlocal content is maximal [9]. When concentrating on quantum evolutions defined by nonlocal Hamiltonians [10], it becomes particularly important to comprehend how the level of nonlocality of the operation influences its capacity for entanglement (i.e., its potential to transition states with a lower degree of entanglement to states with a higher degree of entanglement).

The significance of entanglement in speeding up the dynamical evolutions of composite quantum systems in pure states was initially documented in Refs. [11–13]. Regardless of whether the evolution occurs between orthogonal [11] or nonorthogonal [12] configurations, it has been determined that in the absence of interactions among subsystems, and when the initial state of the composite system is separable, the quantum speed limit can only be attained in the asymmetric scenario where only one of the subsystems undergoes evolution over time and possesses all the energy resources of the system. Conversely, the existence of entanglement in the initial state facilitates a dynamical speedup even when the energy resources are uniformly distributed across the subsystems. In particular, Hamiltonians that generate entanglement can speed up the dynamics, even when beginning from separable configurations [11]. The phenomenon of entanglement accelerating quantum dynamics was further investigated in Refs. [14–19]. In particular, this phenomenon was analyzed for two-qubit systems and systems of two identical bosons in Ref. [14]. Conversely, Ref. [17] examined the relationship between entanglement and the speed of quantum evolution for two quantum particles

in a one-dimensional double well. Although many of these findings are only partially conclusive [20], as they stem from numerical methods and analytic calculations for specific scenarios, the complexity increases for mixed states. For instance, in the case of pure states, a higher degree of entanglement in the initial state correlates with a quicker evolution to an orthogonal state. Nevertheless, in the case of mixed states, there is no conclusive proof that the rate of evolution speeds up solely due to increased entanglement. In fact, the speed may increase with rising entanglement, but this is also observed in other circumstances [21]. In Ref. [22], it was demonstrated that when examining the unitary evolution defined by stationary Hamiltonians of generally mixed states, not all forms of entanglement are beneficial for accelerating time evolution in comparison to non-entangled states. Specifically, it was noted that a significant (time-independent) quantum Fisher information is required to speed up the time evolution relative to non-entangled states. In Ref. [23], the geometric measure of entanglement was associated with the minimum time required to render a pure state separable through a unitary evolution defined by a time-independent nonlocal Hamiltonian. In Ref. [24], the notion of entanglement capacity was established for any bipartite pure state as the variance of the modular Hamiltonian within the reduced state of any subsystem of the composite quantum system. Specifically, it was demonstrated that the quantum speed limit for generating entanglement is influenced not only by the fluctuations in the nonlocal Hamiltonian but also inversely related to the time average of the square root of the entanglement capacity. Lastly, we recommend Refs. [25, 26] for recent compelling studies regarding the speed limit of entanglement dynamics, which is considered the maximum rate at which entanglement can be created or diminished in bipartite quantum systems.

Intriguing studies focusing on linking the geometry of quantum state spaces to entanglement measures defined by negativity, can be found in Refs. [27, 28]. Specifically, when an arbitrary qubit is examined and entanglement is established between the qubit and an ancilla qubit through the application of interaction, the negativity of entanglement is, up to a constant factor, equivalent to the square root of a Riemannian metric. For instance, in the specific case of Ref. [27], the metric in question is the Wigner-Yanase skew-information [29]. In Ref. [30], the geometric characteristics of two-qubit quantum state spaces utilizing the Fubini-Study metric were examined. More precisely, these state spaces were produced through the application of unitary time propagators that correspond to time-independent parametric Hamiltonians acting on specified initial states. Particular attention was given to the impact on the scalar curvature of the state spaces, along with the level of entanglement (measured through the concurrence) of the states. In Ref. [31], the concept of “curvature of entanglement” was characterized as the second derivative of the concurrence with respect to the coupling parameter. This parameter was presumed to be independent of both space and time and, furthermore, delineated the interaction between two qubits. The primary finding of Ref. [31] was a fascinating connection between the instantaneous quantum Fisher information and the curvature of entanglement of a quantum probe characterized by the interaction of two qubits through a Jaynes-Cummings Hamiltonian, while also being influenced by Markovian noise.

Motivated by the complex relationship between nonlocality and entanglement, driven by the absence of a comprehensive geometric description of entanglement in quantum evolutions, and spurred by the increasing interest in linking the geometry of quantum state spaces to measures of entanglement, this paper seeks to investigate the relevant geometric properties of entanglement that emerge from stationary Hamiltonian evolutions transitioning from separable to maximally entangled two-qubit quantum states through the lens of geodesic efficiency [32–34], speed efficiency [35, 36], and the curvature coefficient of quantum evolution [37–39]. A partial list of questions being addressed includes:

- [i] Is it possible to create a parametric family of both optimal and suboptimal stationary Hamiltonians that connect any separable quantum state to a maximally entangled quantum state, given that the evolution is confined to the two-dimensional subspace defined by the source and target states?
- [ii] If suboptimal evolutions with constant Hamiltonians between orthogonal states are not permitted in two dimensions, is it possible to create ad hoc examples of such evolutions in higher-dimensional subspaces of the complete Hilbert space for two-qubit quantum states?
- [iii] In the context of evolutions between identical pairs of separable and maximally entangled quantum states, are time optimal evolutions typically defined by unitary time propagators that exhibit a level of nonlocality exceeding that of their suboptimal counterparts?
- [iv] Do dynamical trajectories that exhibit a higher level of geodesic and speed efficiency also display a greater degree of average path entanglement?
- [v] Do transitions between orthogonal states necessitate greater levels of entanglement in comparison to transitions between nonorthogonal states under the same energy constraints?
- [vi] What are the primary distinctions between suboptimal evolutions in lower-dimensional and higher-dimensional subspaces regarding curvature, energy dissipation, and entanglement capability?

The significance of this analysis is twofold concerning quantum control strategies. Firstly, it broadens the geometric characterization of quantum evolutions by incorporating concepts of efficiency and curvature beyond the dynamics of single qubits, thereby allowing for the examination of the influence of nonlocality and entangling capability on these metrics. Secondly, it provides a framework for comprehending the entanglement properties of both quantum states and unitary time propagators, focusing on their nonlocal characteristics and entangling capabilities, by exploring their interrelationship in connection to their impacts on time-optimality, energy consumption, and curvature of quantum evolutions.

The remainder of this paper is structured as follows. In Section II, we present the fundamental components utilized to characterize the entanglement of a two-qubit quantum state, the nonlocal nature of the unitary time propagator, and its overall ability to generate entanglements from separable states. Specifically, we examine the concepts of concurrence [40], geometric measure of entanglement [41], entanglement production [42], and entangling power [43]. In Section III, we introduce the tools employed to describe certain geometric aspects of quantum evolutions, including geodesic efficiency [32], speed efficiency [35], and curvature coefficient [37, 38]. In Section IV, we present the concepts of time optimal and time suboptimal Hamiltonian evolutions between any pair of quantum states that define any finite-dimensional quantum systems. Notably, we emphasize that while the time optimal scheme is applicable to both orthogonal and nonorthogonal pairs of initial and final states, the suboptimal scheme is limited to pairs of nonorthogonal states. In Section V, concentrating on two-qubit stationary evolutions between separable and maximally entangled states, we investigate four types of Hamiltonian evolutions using both geometric and entanglement quantifiers. The four scenarios we examine are: i) Time optimal evolutions between nonorthogonal quantum states; ii) Time suboptimal quantum evolutions between nonorthogonal states; iii) Time optimal evolutions between orthogonal quantum states; iv) Time suboptimal quantum evolutions between orthogonal states. In Section VI, we focus on links among time optimality, nonlocal character of unitary time propagators, and entanglement capabilities of time optimal evolutions with a different degree of energy wastefulness. Finally, our summary of findings along with our concluding remarks are presented in Section VII.

II. ENTANGLEMENT MEASURES

In this section, we detail the essential elements that we utilize to characterize the entanglement of a two-qubit quantum state, the nonlocal attributes of the unitary time propagator, and its overall capacity to produce entanglements from separable states. In particular, we explore the notions of concurrence, geometric measure of entanglement, entanglement production, and entangling power.

A. Concurrence

To measure the extent of entanglement in a pure two-qubit quantum state $|\psi\rangle$, we employ the concept of concurrence [40, 44, 45]. This measure of entanglement is defined as,

$$C[|\psi\rangle] \stackrel{\text{def}}{=} \langle \psi | \sigma_y \otimes \sigma_y | \psi^* \rangle. \quad (1)$$

It is important to note that $|\psi^*\rangle$ in Eq. (1) represents the complex conjugate of $|\psi\rangle$ within the computational basis, while σ_y refers to the standard Pauli operator. It is noteworthy that if the normalized two-qubit state $|\psi\rangle$ is expressed in terms of the computational basis $\{|00\rangle, |01\rangle, |10\rangle, |11\rangle\}$ as $|\psi\rangle = \alpha|00\rangle + \beta|01\rangle + \gamma|10\rangle + \delta|11\rangle$, the concurrence $C[|\psi\rangle]$ in Eq. (1) simplifies to $C[|\psi\rangle] = 2|\alpha\delta - \beta\gamma|$. Alternatively, if the state $|\psi\rangle$ is reformulated in terms of the magic basis defined as [46]

$$\left\{ |\Phi_1\rangle \stackrel{\text{def}}{=} |\Phi^+\rangle, |\Phi_2\rangle \stackrel{\text{def}}{=} -i|\Phi^-\rangle, |\Phi_3\rangle \stackrel{\text{def}}{=} |\Psi^-\rangle, |\Phi_4\rangle \stackrel{\text{def}}{=} -i|\Psi^+\rangle \right\}, \quad (2)$$

where $|\Phi^\pm\rangle \stackrel{\text{def}}{=} (1/\sqrt{2})(|00\rangle \pm |11\rangle)$ and $|\Psi^\pm\rangle \stackrel{\text{def}}{=} (1/\sqrt{2})(|01\rangle \pm |10\rangle)$ represent the four maximally entangled Bell states, expressed as $|\psi\rangle = \mu_1|\Phi_1\rangle + \mu_2|\Phi_2\rangle + \mu_3|\Phi_3\rangle + \mu_4|\Phi_4\rangle$, the concurrence $C[|\psi\rangle]$ as defined in Eq. (1) simplifies to $C[|\psi\rangle] = |\mu_1^2 + \mu_2^2 + \mu_3^2 + \mu_4^2|$. Furthermore, let us assume that the Schmidt decomposition of $|\psi\rangle$ is provided by

$$|\psi\rangle = \sum_{k=1}^2 \sqrt{\lambda_k} |v_k^{(A)}\rangle \otimes |v_k^{(B)}\rangle, \quad (3)$$

with $\{\sqrt{\lambda_k}\}_{k=1,2}$ representing the Schmidt coefficients, where $\lambda_1 + \lambda_2 = 1$ and $\lambda_k \in \mathbb{R}_+$ for any k . Consequently, for two qubits, the concurrence $C[|\psi\rangle]$ in Eq. (1) simplifies to $C[|\psi\rangle] = 2\Lambda_{\max}\sqrt{1 - \Lambda_{\max}^2}$, where Λ_{\max} denotes the maximum Schmidt coefficient. Notably, $\{\lambda_k\}_{k=1,2}$ are the eigenvalues of the reduced density operators $\rho_A = \text{Tr}_B(|\psi\rangle\langle\psi|)$ and $\rho_B = \text{Tr}_A(|\psi\rangle\langle\psi|)$. Lastly, it is important to mention that the number of terms in the expansion in Eq. (3) is referred to as the Schmidt number. For a separable state, the Schmidt number is consistently 1. In contrast, an entangled state has a Schmidt number greater than 1.

In the next subsection, we introduce an alternative measure of entanglement of pure states.

B. Geometric measure of entanglement

The geometric measure of entanglement for pure states, as introduced by Shimony in Ref. [41], employs fundamental concepts of Hilbert space geometry to assess the extent of entanglement in pure states. It is characterized as the minimal squared distance between an entangled state $|\psi\rangle$ and the collection of separable states $|\phi\rangle$,

$$E_{\text{geo}}[|\psi\rangle] \stackrel{\text{def}}{=} \min_{|\phi\rangle} \||\psi\rangle - |\phi\rangle\|^2. \quad (4)$$

With respect to the squared Fubini-Study distance [47], $E_{\text{geo}}[|\psi\rangle]$ in Eq. (4) can be reformulated as

$$E_{\text{geo}}[|\psi\rangle] = \min_{|\phi\rangle} \left[1 - |\langle\psi|\phi\rangle|^2 \right] = 1 - \max_{|\phi\rangle} \left[|\langle\psi|\phi\rangle|^2 \right]. \quad (5)$$

Although its definition is straightforward, calculating $E_{\text{geo}}[|\psi\rangle]$ in Eq.(5) necessitates a complex minimization process across all separable states. Notably, when we define the entanglement eigenvalue Λ_{\max} as $\Lambda_{\max} \stackrel{\text{def}}{=} \max_{|\phi\rangle} |\langle\psi|\phi\rangle|$, it is revealed that for bipartite systems, Λ_{\max} corresponds to the largest Schmidt coefficient found in the Schmidt decomposition of $|\psi\rangle$ [48]. Consequently, in this scenario, $E_{\text{geo}}[|\psi\rangle]$ simplifies to $E_{\text{geo}}[|\psi\rangle] = 1 - \Lambda_{\max}^2$. Lastly, considering that the concurrence $C[|\psi\rangle]$ of $|\psi\rangle$ is represented as $2\Lambda_{\max}\sqrt{1 - \Lambda_{\max}^2}$, the connection between $E_{\text{geo}}[|\psi\rangle]$ and $C[|\psi\rangle]$ is expressed as $E_{\text{geo}}[|\psi\rangle] = (1/2) \left[1 - \sqrt{1 - C^2[|\psi\rangle]} \right]$.

Considering the evident connection between concurrence and the geometric measure of entanglement, we will utilize concurrence to quantify the degree of entanglement in a pure state in the subsequent sections. Conversely, in the following subsection, we will introduce an entanglement measure that is appropriate for assessing the propensity of an operator to produce entangled states from separable states.

C. Entanglement production

In the following subsection, we will provide a brief introduction to the concept of entanglement production, as originally presented by Yukalov and collaborators in Refs. [42, 49–51]. Specifically, our focus here will be on Ref. [42]. We will examine a bipartite quantum system defined by the Hilbert space $\mathcal{H} \stackrel{\text{def}}{=} \mathcal{H}_A \otimes \mathcal{H}_B$, where $\mathcal{H}_A \stackrel{\text{def}}{=} \text{Span}\{|n\rangle\}_{n=1, \dots, n_A}$, $\mathcal{H}_B \stackrel{\text{def}}{=} \text{Span}\{|\alpha\rangle\}_{\alpha=1, \dots, n_B}$, and $\mathcal{H} \stackrel{\text{def}}{=} \text{Span}\{|n\rangle \otimes |\alpha\rangle\}_{n=1, \dots, n_A}^{\alpha=1, \dots, n_B}$. The dimensions are given by $\dim \mathcal{H}_A \stackrel{\text{def}}{=} n_A$, $\dim \mathcal{H}_B \stackrel{\text{def}}{=} n_B$, and $\dim \mathcal{H} \stackrel{\text{def}}{=} n_A n_B$. We will consider a unitary evolution operator represented by $U(t) = e^{-\frac{i}{\hbar}Ht}$ that operates on $\mathcal{H} \stackrel{\text{def}}{=} \mathcal{H}_A \otimes \mathcal{H}_B$, where H denotes a time-independent Hamiltonian for the composite quantum system. Consequently, the entanglement production of $U(t)$ is defined as

$$\varepsilon_{\text{EP}}^{\text{Yukalov}}[U(t)] \stackrel{\text{def}}{=} \log \left[\frac{\|U(t)\|}{\|U^\otimes(t)\|} \right], \quad (6)$$

where $\|U(t)\|$ is the Hilbert-Schmidt norm of $U(t)$ given by $\|U(t)\| \stackrel{\text{def}}{=} \sqrt{\text{Tr}_{\mathcal{H}}[U^\dagger(t)U(t)]}$. To ensure thoroughness, we highlight that $\|U(t)\|$ is equal to one for unitary operators $U(t)$. Nevertheless, the definition of $\varepsilon_{\text{EP}}^{\text{Yukalov}}[U(t)]$ is applicable to broader scenarios where unitarity is not a strict requirement. The so-called nonentangling operator $U^\otimes(t)$ in Eq. (6) is defined as

$$U^\otimes(t) \stackrel{\text{def}}{=} \frac{U_A(t) \otimes U_B(t)}{\text{Tr}_{\mathcal{H}}[U(t)]} = \frac{\text{Tr}_{\mathcal{H}_B}[U(t)] \otimes \text{Tr}_{\mathcal{H}_A}[U(t)]}{\text{Tr}_{\mathcal{H}}[U(t)]}. \quad (7)$$

Operator, U	Weyl chamber location, (c_1, c_2, c_3)	Entangling power, $\varepsilon_{\text{EP}}^{\text{Zanardi}}(U)$	Schmidt number, $\text{Sch}(U)$
Identity	$(0, 0, 0)$	0	1
CNOT	$(\pi/4, 0, 0)$	$2/9$	2
SWAP	$(\pi/4, \pi/4, \pi/4)$	0	4
$\sqrt{\text{SWAP}}$	$(\pi/8, \pi/8, \pi/8)$	$1/6$	2
DCNOT	$(\pi/4, \pi/4, 0)$	$2/9$	4

TABLE I: Tabular summary illustrating the the Weyl chamber position, the entangling capability, and the Schmidt number associated with standard two-qubit quantum gates.

The operators $U_A(t)$ and $U_B(t)$ in Eq. (7) are the partial evolution operators used to construct the nonentangling operator $U^\otimes(t)$. Note that the logarithm in Eq. (6) can be taken with respect to any convenient base.

More broadly, the concept underlying the definition of this measure in Eq. (6) is to evaluate the action of a specific operator A in comparison to that of its non-entangling equivalent A^\otimes . A non-entangling operator applied to a subset \mathcal{D} of the complete Hilbert space \mathcal{H} is defined as an operator that transforms any separable state within \mathcal{D} into a separable state also within $\mathcal{D} \subseteq \mathcal{H}$. Conversely, an entangling operator on \mathcal{D} is characterized by the existence of at least one element in \mathcal{D} that is transformed into an entangled state in $\mathcal{H} \setminus \mathcal{D}$. A universal entangling operator on \mathcal{D} is defined as one that causes any element of \mathcal{D} to become entangled when acted upon by the universal entangling operator. It is evident that the SWAP operator and tensor products of local operators serve as examples of operators that maintain separability. The idea of establishing this measure for entanglement production in Eq. (6) stems from the notion of operator order indices within the realm of statistical mechanics [52, 53]. These indices are articulated through the norms of operators. Furthermore, given that the order structure of composite quantum systems displaying interparticle correlations aligns well with entangled systems, entanglement production was initially introduced by Yukalov in Ref. [49]. Considering the difference between the “static” concepts of state entanglement and the nonlocal characteristics of an operator, Yukalov’s concept of entanglement production is a “dynamic” idea that illustrates how an operator can generate entangled states from separable ones. Its operational significance demonstrates the capacity of an operator to create entangled state vectors within the Hilbert space on which it operates. This concept is not restricted to unitary operators, bipartite systems, and pure states; rather, it also encompasses nonunitary operators, multipartite systems, and mixed states. The measure of entanglement production is zero for non entangling operators. Furthermore, it is continuous in terms of norm convergence, additive, invariant under local unitary transformations, and semipositive. In particular, the characteristics of the Hilbert-Schmidt norm play an important role in demonstrating that the entanglement production meets all the fundamental criteria of a well-defined entanglement measure. For completeness, we point out here that the Hilbert-Schmidt norm of operators is extensively utilized in the literature for characterizing entanglement [54–58]. For example, in Ref. [54], the Hilbert-Schmidt entanglement of a state is defined as the minimum distance, as determined by the Hilbert-Schmidt norm, between the density matrix representing the state and the collection of all disentangled states. Due to the practical challenges associated with calculating the values of most entanglement measures, Ref. [57] employed the Hilbert-Schmidt distance to develop an entanglement witness aimed at simply certifying the presence of entanglement in the state, while disregarding its specific entanglement content. For further details on entanglement production, we suggest Refs. [42, 49–51].

In the next subsection, we introduce an alternative to Yukalov’s entanglement production.

D. Entangling power

Zanardi’s entangling power defines the entangling ability of unitary operators. It is characterized as the average entanglement that the unitary operator can generate when applied to all separable states, which are distributed according to a specific probability density over the manifold of product states.

Consider a bipartite quantum system characterized by the state space $\mathcal{H} = \mathcal{H}_A \otimes \mathcal{H}_B$, where $\dim_{\mathbb{C}} \mathcal{H}_A = d_A$ and $\dim_{\mathbb{C}} \mathcal{H}_B = d_B$. Note that the subscript “ \mathbb{C} ” denotes the field of complex numbers. Let U represent a unitary operator that acts on \mathcal{H} , and let \mathcal{E} denote an entanglement measure defined over \mathcal{H} . Consequently, in relation to \mathcal{E} , the entangling power of U is defined as

$$\varepsilon_{\text{EP}}^{\text{Zanardi}}(U) \stackrel{\text{def}}{=} \overline{\mathcal{E}[U(|\psi_A\rangle \otimes |\psi_B\rangle)]}, \quad (8)$$

where the bar in Eq. (8) signifies the average across all product states $|\psi_A\rangle \otimes |\psi_B\rangle$ that are distributed according to a certain probability density $p = p(|\psi_A\rangle, |\psi_B\rangle)$ over the manifold of product states [43, 59, 60]. The selected

Quantum Gate, U	Entangling power, $\varepsilon_{\text{EP}}^{\text{Zanardi}}(U)$	Nonlocal character	Schmidt number, $\text{Sch}(U)$
SWAP	No, 0	Yes, maximal	4
DCNOT	Yes, 2/9	Yes, maximal	4
CNOT	Yes, 2/9	Yes, non-maximal	2

TABLE II: A schematic overview of the entangling capabilities, nonlocal properties, and Schmidt number associated with the SWAP, DCNOT, and CNOT gates is presented. It is important to highlight that the SWAP gate demonstrates no entangling power, even though it displays a maximal nonlocal character. Furthermore, both the DCNOT and CNOT gates exhibit identical entangling power, despite having distinct levels of nonlocal character.

entanglement measure for $|\psi\rangle \in \mathcal{H}$ is the linear entropy $\mathcal{E} [|\psi\rangle]$ defined as $\mathcal{E} [|\psi\rangle] \stackrel{\text{def}}{=} 1 - \text{Tr} [\rho_A^2] = 1 - \text{Tr} [\rho_B^2]$, where $\rho_A \stackrel{\text{def}}{=} \text{Tr}_B [|\psi\rangle \langle \psi|]$ and $\rho_B \stackrel{\text{def}}{=} \text{Tr}_A [|\psi\rangle \langle \psi|]$. It is important to note that $\mathcal{E} [|\psi\rangle]$ quantifies the purity of the reduced density matrix ρ_A .

For systems involving two qubits, any unitary operator U belonging to $\text{SU}(4)$ can be expressed in a canonical form as [61, 62]

$$U = (A_1 \otimes B_1) e^{-i(c_1 \sigma_1 \otimes \sigma_1 + c_2 \sigma_2 \otimes \sigma_2 + c_3 \sigma_3 \otimes \sigma_3)} (A_2 \otimes B_2), \quad (9)$$

where $\boldsymbol{\sigma} \stackrel{\text{def}}{=} (\sigma_1, \sigma_2, \sigma_3)$ is the vector of Pauli spin matrices, and $A_i, B_i \in \text{SU}(2)$ are single-qubit unitary operators. Interestingly, two operators U_1 and $U_2 \in \text{SU}(4)$ are locally equivalent if there exist some single-qubit unitary operators $\tilde{A}_1, \tilde{B}_1, \tilde{A}_2, \tilde{B}_2$ such that

$$U_2 = (\tilde{A}_1 \otimes \tilde{B}_1) U_1 (\tilde{A}_2 \otimes \tilde{B}_2). \quad (10)$$

From Eqs. (9) and (10), it can be inferred that any operator within $\text{SU}(4)$ is locally equivalent to $e^{-i(c_1 \sigma_1 \otimes \sigma_1 + c_2 \sigma_2 \otimes \sigma_2 + c_3 \sigma_3 \otimes \sigma_3)}$ for an appropriate selection of the geometrical point that defines the two-qubit gate in the Weyl chamber, where $c_1 \geq c_2 \geq c_3 \geq 0$. In the standard computational basis, the matrix representation of $e^{-i(c_1 \sigma_1 \otimes \sigma_1 + c_2 \sigma_2 \otimes \sigma_2 + c_3 \sigma_3 \otimes \sigma_3)}$ is expressed as

$$U = \begin{pmatrix} e^{-ic_3} c_- & 0 & 0 & -ie^{-ic_3} s_- \\ 0 & e^{ic_3} c_+ & -ie^{ic_3} s_- & 0 \\ 0 & -ie^{ic_3} s_- & e^{ic_3} c_+ & 0 \\ -ie^{-ic_3} s_- & 0 & 0 & e^{-ic_3} c_- \end{pmatrix}, \quad (11)$$

where $c_{\pm} \stackrel{\text{def}}{=} \cos(c_1 \pm c_2)$ and $s_{\pm} \stackrel{\text{def}}{=} \sin(c_1 \pm c_2)$. It has been determined that the entangling power $\varepsilon(U)$ as stated in Eq. (8) for the unitary U presented in Eq. (11) is equivalent to [61, 62],

$$\varepsilon_{\text{EP}}^{\text{Zanardi}}(U) = \frac{1}{18} \{3 - [\cos(4c_1) \cos(4c_2) + \cos(4c_2) \cos(4c_3) + \cos(4c_3) \cos(4c_1)]\}, \quad (12)$$

where it can be noted that $\varepsilon(U)$ is determined solely by the non-local component of U , which is defined through the vector $\mathbf{c} \stackrel{\text{def}}{=} (c_1, c_2, c_3)$. In Table I, we present a tabular summary that illustrates the Weyl chamber position, the entangling capability, and the Schmidt number related to standard two-qubit quantum gates. In Table II, on the other hand, we provide a schematic overview of the entangling capabilities, nonlocal properties, and Schmidt number associated with the SWAP, DCNOT, and CNOT gates [63]. It is crucial to emphasize that the SWAP gate shows no entangling power, despite exhibiting a maximal nonlocal character. Moreover, both the DCNOT and CNOT gates display the same entangling power, even though they possess different levels of nonlocal character.

After discussing both static and dynamic entanglement quantifiers, we will now present the measures we employ to describe quantum evolutions from a geometric perspective.

III. GEOMETRIC ASPECTS OF QUANTUM EVOLUTIONS

In this section, we present the tools utilized to articulate certain geometric features of quantum evolutions, which encompass geodesic efficiency, speed efficiency, and curvature coefficient.

A. Efficiency

1. Geodesic efficiency

We start with the concept of geodesic efficiency. Examine the progression of a state vector $|\psi(t)\rangle$ as articulated by the time-dependent Schrödinger equation, $i\hbar\partial_t|\psi(t)\rangle = H(t)|\psi(t)\rangle$, over the interval $t_A \leq t \leq t_B$. As a result, the geodesic efficiency η_{GE} for this quantum evolution is a scalar value that remains invariant over time (global) and is characterized within the limits of $0 \leq \eta_{\text{GE}} \leq 1$. This is defined as [32, 64]

$$\eta_{\text{GE}} \stackrel{\text{def}}{=} \frac{s_0}{s} = \frac{2 \arccos [|\langle A | B \rangle|]}{2 \int_{t_A}^{t_B} \frac{\Delta E(t)}{\hbar} dt}. \quad (13)$$

The quantity s_0 denotes the distance along the shortest geodesic path that links the initial state $|A\rangle \stackrel{\text{def}}{=} |\psi(t_A)\rangle$ to the final state $|B\rangle \stackrel{\text{def}}{=} |\psi(t_B)\rangle$ within the complex projective Hilbert space. Furthermore, the quantity s in Eq. (13) represents the distance along the dynamical trajectory $\gamma(t) : t \mapsto |\psi(t)\rangle$ that corresponds to the evolution of the state vector $|\psi(t)\rangle$ for $t_A \leq t \leq t_B$. It is evident that a geodesic quantum evolution characterized by $\gamma(t) = \gamma_{\text{geo}}(t)$ is defined by the equation $\eta_{\text{GE}}^{(\gamma_{\text{geo}})} = 1$. The term $\Delta E(t) \stackrel{\text{def}}{=} [\langle \psi | H^2(t) | \psi \rangle - \langle \psi | H(t) | \psi \rangle^2]^{1/2}$ indicates the energy uncertainty of the system, expressed as the square root of the dispersion of $H(t)$. Importantly, Anandan and Aharonov established that the infinitesimal distance $ds \stackrel{\text{def}}{=} 2[\Delta E(t)/\hbar]dt$ is connected to the Fubini-Study infinitesimal distance ds_{FS} through the relationship [32],

$$ds_{\text{FS}}^2 (|\psi(t)\rangle, |\psi(t+dt)\rangle) \stackrel{\text{def}}{=} 4 \left[1 - |\langle \psi(t) | \psi(t+dt) \rangle|^2 \right] = 4 \frac{\Delta E^2(t)}{\hbar^2} dt^2 + \mathcal{O}(dt^3), \quad (14)$$

with $\mathcal{O}(dt^3)$ being an infinitesimal term of an order that equals or is greater than dt^3 . From the connection between ds_{FS} and ds , it can be inferred that s is directly proportional to the time integral of ΔE . Additionally, s denotes the distance computed using the Fubini-Study metric during the evolution of the quantum system in ray space (i.e., the projective Hilbert space $\mathcal{P}(\mathcal{H})$ of a complex Hilbert space \mathcal{H} defined by the set of equivalence classes of non-zero state vectors in \mathcal{H} [32]). It is crucial to highlight that when the actual dynamical trajectory aligns with the shortest geodesic path linking $|A\rangle$ and $|B\rangle$, s is equivalent to s_0 , and the geodesic efficiency η_{GE} in Eq. (13) is equal to one. Clearly, π (i.e., $2 \arccos(0)$) signifies the minimal distance separating two orthogonal pure states in ray space.

2. Speed efficiency

We proceed here with the concept of speed efficiency. We start by recalling that appropriate families of nonstationary Hamiltonians capable of generating predetermined dynamical trajectories with minimal energy resource expenditure were first introduced in Ref. [35]. While these trajectories are energy-efficient, they do not usually correspond to geodesic paths of the shortest length. The criterion for minimal energy expenditure is met when no energy is wasted on segments of the Hamiltonian $H = H(t)$ that do not effectively direct the system. In other words, all available energy, as represented by the spectral norm of the Hamiltonian $\|H\|_{\text{SP}}$, is transformed into the system's evolution speed $v_H(t) \stackrel{\text{def}}{=} (2/\hbar)\Delta E(t)$, where $\Delta E(t)$ signifies the energy uncertainty.

More specifically, Uzdin's speed efficiency η_{SE} in Ref. [35] denotes a time-dependent (local) scalar quantity that fulfills the condition $0 \leq \eta_{\text{SE}} \leq 1$. It is identified as

$$\eta_{\text{SE}}(t) \stackrel{\text{def}}{=} \frac{\Delta H_\rho}{\|H\|_{\text{SP}}} = \frac{\sqrt{\text{tr}(\rho H^2) - [\text{tr}(\rho H)]^2}}{\max \left[\sqrt{\text{eig}(H^\dagger H)} \right]}. \quad (15)$$

While $\Delta H_\rho = \Delta E(t)$ and $\rho = \rho(t)$ denotes the density operator that defines the quantum system at time t , the quantity $\|H\|_{\text{SP}}$ present in the denominator of Eq. (15) is given by $\|H\|_{\text{SP}} \stackrel{\text{def}}{=} \max \left[\sqrt{\text{eig}(H^\dagger H)} \right]$. Note that if H is Hermitian, $\|H\|_{\text{SP}}$ is simply the magnitude of the maximum-magnitude eigenvalue of H . This quantity is referred to as the spectral norm $\|H\|_{\text{SP}}$ of the Hamiltonian operator H , which acts as a measure of the magnitude of bounded linear operators. It is computed as the square root of the maximum eigenvalue of the operator $H^\dagger H$, with H^\dagger representing the Hermitian conjugate of H .

After implementing methods to measure the length and energy dissipation of dynamical trajectories, we will detail in the following subsection how these trajectories "bend" during quantum evolutions.

B. Curvature

In the broadest context, we examine a nonstationary Hamiltonian evolution as described by Schrödinger's equation $i\hbar\partial_t |\psi(t)\rangle = H(t)|\psi(t)\rangle$, where $|\psi(t)\rangle$ represents an element within an arbitrary N -dimensional complex Hilbert space \mathcal{H}_N . Typically, the normalized state vector $|\psi(t)\rangle$ adheres to the condition $\langle\psi(t)|\dot{\psi}(t)\rangle = (-i/\hbar)\langle\psi(t)|H(t)|\psi(t)\rangle \neq 0$. For the state $|\psi(t)\rangle$, we introduce the parallel transported unit state vector $|\Psi(t)\rangle \stackrel{\text{def}}{=} e^{i\beta(t)}|\psi(t)\rangle$, with the phase $\beta(t)$ defined such that $\langle\Psi(t)|\dot{\Psi}(t)\rangle = 0$. It is important to note that $i\hbar\langle\dot{\Psi}(t)\rangle = [H(t) - \hbar\dot{\beta}(t)]|\Psi(t)\rangle$. As a result, the condition $\langle\Psi(t)|\dot{\Psi}(t)\rangle = 0$ is equivalent to establishing $\beta(t)$ as $\beta(t) \stackrel{\text{def}}{=} (1/\hbar)\int_0^t \langle\psi(t')|H(t')|\psi(t')\rangle dt'$. Therefore, $|\Psi(t)\rangle$ can be simplified to

$$|\Psi(t)\rangle = e^{(i/\hbar)\int_0^t \langle\psi(t')|H(t')|\psi(t')\rangle dt'}|\psi(t)\rangle, \quad (16)$$

and satisfies the evolution equation $i\hbar\langle\dot{\Psi}(t)\rangle = \Delta H(t)|\Psi(t)\rangle$ where $\Delta H(t) \stackrel{\text{def}}{=} H(t) - \langle H(t)\rangle$. It is important to note that the speed $v(t)$ of quantum evolution changes when the Hamiltonian is time-dependent. Specifically, $v(t)$ is defined such that $v^2(t) = \langle\dot{\Psi}(t)|\dot{\Psi}(t)\rangle = \langle(\Delta H(t))^2\rangle/\hbar^2$. For ease of reference, we define the arc length $s = s(t)$ in relation to $v(t)$ as $s(t) \stackrel{\text{def}}{=} \int_0^t v(t')dt'$, with $ds = v(t)dt$ (which consequently indicates that $\partial_t = v(t)\partial_s$), where $\partial_t \stackrel{\text{def}}{=} \partial/\partial t$ and $\partial_s \stackrel{\text{def}}{=} \partial/\partial s$. In summary, by introducing the dimensionless operator

$$\Delta h(t) \stackrel{\text{def}}{=} \frac{\Delta H(t)}{\hbar v(t)} = \frac{\Delta H(t)}{\sqrt{\langle(\Delta H(t))^2\rangle}}, \quad (17)$$

the normalized tangent vector $|T(s)\rangle \stackrel{\text{def}}{=} \partial_s|\Psi(s)\rangle = |\Psi'(s)\rangle$ becomes $|T(s)\rangle = -i\Delta h(s)|\Psi(s)\rangle$. It is crucial to acknowledge that $\langle T(s)|T(s)\rangle = 1$ by construction. Additionally, we have $\partial_s\langle\Delta h(s)\rangle = \langle\Delta h'(s)\rangle$. From the tangent vector $|T(s)\rangle = -i\Delta h(s)|\Psi(s)\rangle$, we can derive $|T'(s)\rangle \stackrel{\text{def}}{=} \partial_s|T(s)\rangle$. Through algebraic manipulation, we find that $|T'(s)\rangle = -i\Delta h(s)|\Psi'(s)\rangle - i\Delta h'(s)|\Psi(s)\rangle$, where $\langle T'(s)|T'(s)\rangle = \langle(\Delta h'(s))^2\rangle + \langle(\Delta h(s))^4\rangle - 2i\text{Re}[\langle\Delta h'(s)(\Delta h(s))^2\rangle] \neq 1$ in most instances. We are now prepared to introduce the curvature coefficient for quantum evolutions generated by nonstationary Hamiltonians.

Following the introduction of the vectors $|\Psi(s)\rangle$, $|T(s)\rangle$, and $|T'(s)\rangle$, we are now able to define the curvature coefficient as initially outlined in Refs. [37, 38, 65]. This coefficient is represented as $\kappa_{\text{AC}}^2(s) \stackrel{\text{def}}{=} \langle\tilde{N}_*(s)|\tilde{N}_*(s)\rangle$. It is essential to recognize that $|\tilde{N}_*(s)\rangle \stackrel{\text{def}}{=} P^{(\Psi)}|T'(s)\rangle$, where the projection operator $P^{(\Psi)}$ onto states orthogonal to $|\Psi(s)\rangle$ is given by $P^{(\Psi)} \stackrel{\text{def}}{=} I - |\Psi(s)\rangle\langle\Psi(s)|$. In this context, “I” denotes the identity operator in \mathcal{H}_N . The subscript “AC” signifies Alsing and Cafaro. It is significant to mention that the curvature coefficient $\kappa_{\text{AC}}^2(s) = \langle\tilde{N}_*(s)|\tilde{N}_*(s)\rangle$ can be expressed in a more convenient form as

$$\kappa_{\text{AC}}^2(s) \stackrel{\text{def}}{=} \|D|T(s)\rangle\|^2 = \|D^2|\Psi(s)\rangle\|^2, \quad (18)$$

where $D \stackrel{\text{def}}{=} P^{(\Psi)}d/ds = (I - |\Psi(s)\rangle\langle\Psi(s)|)d/ds$ such that $D|T(s)\rangle \stackrel{\text{def}}{=} P^{(\Psi)}|T'(s)\rangle = |\tilde{N}_*(s)\rangle$ is the covariant derivative [33, 66, 67]. As stated in Eq. (18), the curvature coefficient $\kappa_{\text{AC}}^2(s)$ is found to be equivalent to the square of the magnitude of the second covariant derivative of the state vector $|\Psi(s)\rangle$, which delineates the quantum Schrödinger trajectory in the context of projective Hilbert space.

Ultimately, an expression that demonstrates computational efficiency for the curvature coefficient $\kappa_{\text{AC}}^2(s)$ in Eq. (18) within any arbitrary nonstationary context is reduced to

$$\kappa_{\text{AC}}^2(s) = \langle(\Delta h)^4\rangle - \langle(\Delta h)^2\rangle^2 + \left[\langle(\Delta h')^2\rangle - \langle\Delta h'\rangle^2\right] + i\langle[(\Delta h)^2, \Delta h']\rangle. \quad (19)$$

From Eq. (19), it is noted that when the Hamiltonian H is held constant, $\Delta h'$ becomes the null operator, enabling us to obtain the stationary limit $\langle(\Delta h)^4\rangle - \langle(\Delta h)^2\rangle^2$ for the curvature coefficient $\kappa_{\text{AC}}^2(s)$ [37]. The expression for $\kappa_{\text{AC}}^2(s)$ in Eq. (19) is formulated through a method that relies on the calculation of expectation values, which require

a comprehension of the state vector $|\psi(t)\rangle$ governed by the time-dependent Schrödinger's evolution equation. As elaborated in Ref. [38], this methodology of expectation values offers a significant statistical meaning for $\kappa_{AC}^2(s)$.

We are now prepared to introduce appropriate Hamiltonian models to which the entanglement and geometric evolution quantifiers discussed in Sections II and III, respectively, can be applied.

IV. HAMILTONIAN MODELS

In this section, we present the concepts of time optimal and time suboptimal Hamiltonian evolutions applicable to any pair of quantum states that define finite-dimensional quantum systems.

A. Time optimal Hamiltonians

In accordance with Refs. [33, 68], we consider a traceless and stationary Hamiltonian H characterized by a spectral decomposition expressed as $H \stackrel{\text{def}}{=} E_1 |E_1\rangle\langle E_1| + E_2 |E_2\rangle\langle E_2|$, where $\langle E_1|E_2\rangle = \delta_{12}$ and $E_2 \geq E_1$. For the sake of transparency, it is important to note that the sets $\{|E_i\rangle\}_{i=1,2}$ and $\{E_i\}_{i=1,2}$ represent the eigenvectors and eigenvalues of the constant Hamiltonian H , respectively. Additionally, δ_{ij} signifies the Kronecker delta symbol, applicable for $1 \leq i, j \leq 2$. In scenarios that are time-optimal, the focus is on the evolution of a state $|A\rangle$, which may not be normalized, into a state $|B\rangle$ in the least amount of time by maximizing the energy uncertainty ΔE ,

$$\Delta E \stackrel{\text{def}}{=} \left[\frac{\langle A|H^2|A\rangle}{\langle A|A\rangle} - \left(\frac{\langle A|H|A\rangle}{\langle A|A\rangle} \right)^2 \right]^{1/2}, \quad (20)$$

in such a manner that ΔE in Eq. (20) is equal to ΔE_{\max} . The rationale behind maximizing the energy uncertainty ΔE is based on the observation that the rate of quantum evolution ds/dt along the trajectory connecting $|A\rangle$ to $|B\rangle$ is directly proportional to the energy uncertainty ΔE , expressed as $ds/dt \propto \Delta E$. What is the maximum value of ΔE_{\max} ? To determine this value, we recognize that any unnormalized initial state $|A\rangle$ can be expressed as $|A\rangle = \alpha_1 |E_1\rangle + \alpha_2 |E_2\rangle$, where α_1 and α_2 are generally complex quantum amplitudes defined as $\alpha_1 \stackrel{\text{def}}{=} \langle E_1|A\rangle$ and $\alpha_2 \stackrel{\text{def}}{=} \langle E_2|A\rangle$. By substituting this decomposition of $|A\rangle$ into Eq. (20), we obtain

$$\Delta E = \frac{E_2 - E_1}{2} \left[1 - \left(\frac{|\alpha_1|^2 - |\alpha_2|^2}{|\alpha_1|^2 + |\alpha_2|^2} \right)^2 \right]^{1/2}. \quad (21)$$

An examination of Eq. (21) indicates that the peak value of ΔE in Eq. (21) occurs when $|\alpha_1| = |\alpha_2|$. Specifically, it is equal to

$$\Delta E_{\max} \stackrel{\text{def}}{=} \left(\frac{E_2 - E_1}{2} \right). \quad (22)$$

A key principle in Mostafazadeh's methodology, as outlined in Ref. [68], is the representation of $H \stackrel{\text{def}}{=} E_1 |E_1\rangle\langle E_1| + E_2 |E_2\rangle\langle E_2|$ in relation to the initial and final states $|A\rangle$ and $|B\rangle$, respectively, while ensuring that $\Delta E = \Delta E_{\max}$. In this framework, it is crucial to acknowledge that $|A\rangle$ and $|B\rangle$ can be represented as $|A\rangle = \alpha_1 |E_1\rangle + \alpha_2 |E_2\rangle$ and $|B\rangle = \beta_1 |E_1\rangle + \beta_2 |E_2\rangle$, respectively. Additionally, it is essential to enforce $|\alpha_1| = |\alpha_2|$ and $|\beta_1| = |\beta_2|$ or, alternatively,

$$|\alpha_2|^2 - |\alpha_1|^2 = 0 = |\beta_2|^2 - |\beta_1|^2, \quad (23)$$

to satisfy the condition $\Delta E = \Delta E_{\max}$ and consequently guarantee the minimum travel time $t_{AB}^{\min} \stackrel{\text{def}}{=} \hbar \arccos(|\langle A|B\rangle|) / \Delta E_{\max}$. After performing some straightforward yet tedious algebra, one can demonstrate that the expression for the time-optimal Hamiltonian H , which links $|A\rangle$ to $|B\rangle$ (assuming energy dispersion $\Delta E = E$, with $E_2 = -E_1 = E$), is provided by [33]

$$H_{\text{opt}} \stackrel{\text{def}}{=} i\Delta E \frac{|\langle A|B\rangle|}{\sqrt{1 - |\langle A|B\rangle|^2}} \left[\frac{|B\rangle\langle A|}{\langle A|B\rangle} - \frac{|A\rangle\langle B|}{\langle B|A\rangle} \right]. \quad (24)$$

Recalling that quantum states differing only by a global phase are physically indistinguishable, we emphasize for thoroughness that the unitary time propagator $U_{\text{opt}}(t) \stackrel{\text{def}}{=} e^{-\frac{i}{\hbar} H_{\text{opt}} t}$ satisfies $U_{\text{opt}}(t_{\text{opt}}) |A\rangle = |B\rangle$ with $t_{\text{opt}} = t_{AB}^{\min}$ defined as

$$t_{\text{opt}} \stackrel{\text{def}}{=} \frac{\hbar \arccos(|\langle A | B \rangle|)}{\Delta E}. \quad (25)$$

In conclusion, we note that for H_{opt} as presented in Eq. (24), it is correctly derived that $\langle A | H_{\text{opt}} | A \rangle / \langle A | A \rangle = 0$ and $\Delta E = [\langle A | H_{\text{opt}}^2 | A \rangle / \langle A | A \rangle]^{1/2} = E = \Delta E_{\text{max}}$.

Having covered the fundamentals of constructing optimal-time Hamiltonians, we are now ready to investigate deviations from time-optimality in two-dimensional subspaces.

B. Time suboptimal Hamiltonians

In the following discussion, we develop a one-parameter family of time suboptimal, time-independent Hamiltonians that connect two arbitrary nonorthogonal quantum states within any finite-dimensional quantum system. It is important to note that regarding the eigenvectors of the Hamiltonian, the initial and final states $|A\rangle$ and $|B\rangle$ can be expressed as $|A\rangle = \alpha_1 |E_1\rangle + \alpha_2 |E_2\rangle$, and $|B\rangle = \beta_1 |E_1\rangle + \beta_2 |E_2\rangle$, respectively. To guarantee a non-minimum travel time $t_{AB} \geq t_{AB}^{\min}$ while maintaining ΔE at a value consistently less than its maximum ΔE_{max} , we establish $\delta |\alpha_1| = |\alpha_2|$, and $\delta |\beta_1| = |\beta_2|$. Consequently, we define $\alpha_2 \stackrel{\text{def}}{=} e^{i\varphi_\alpha} \delta \alpha_1$ and, $\beta_2 \stackrel{\text{def}}{=} e^{i\varphi_\beta} \delta \beta_1$, with $\delta \in \mathbb{R}_+ \setminus \{0\}$. Then, $|A\rangle$ and $|B\rangle$ can be expressed as

$$|A\rangle = \alpha_1 |E_1\rangle + \alpha_2 |E_2\rangle = \alpha_1 |E_1\rangle + e^{i\varphi_\alpha} \delta \alpha_1 |E_2\rangle, \text{ and } |B\rangle = \beta_1 |E_1\rangle + \beta_2 |E_2\rangle = \beta_1 |E_1\rangle + e^{i\varphi_\beta} \delta \beta_1 |E_2\rangle, \quad (26)$$

respectively. From Eq. (26), we conveniently introduce the normalized states $|\mathcal{A}\rangle$ and $|\mathcal{B}\rangle$ such that

$$|E_1\rangle + e^{i\varphi_\alpha} \delta |E_2\rangle = \alpha_1^{-1} |A\rangle \stackrel{\text{def}}{=} \sqrt{1 + \delta^2} |\mathcal{A}\rangle, \text{ and } |E_1\rangle + e^{i\varphi_\beta} \delta |E_2\rangle = \beta_1^{-1} |B\rangle \stackrel{\text{def}}{=} \sqrt{1 + \delta^2} e^{-i\frac{\varphi_\alpha - \varphi_\beta}{2}} |\mathcal{B}\rangle, \quad (27)$$

that is,

$$|\mathcal{A}\rangle \stackrel{\text{def}}{=} \frac{1}{\sqrt{1 + \delta^2}} [|E_1\rangle + e^{i\varphi_\alpha} \delta |E_2\rangle], \text{ and } |\mathcal{B}\rangle \stackrel{\text{def}}{=} \frac{1}{\sqrt{1 + \delta^2}} \left[e^{i\frac{\varphi_\alpha - \varphi_\beta}{2}} |E_1\rangle + e^{i\frac{\varphi_\alpha + \varphi_\beta}{2}} \delta |E_2\rangle \right]. \quad (28)$$

Evidently, the matrix representation illustrating the relationships between the sets of states $\{|\mathcal{A}\rangle, |\mathcal{B}\rangle\}$ and $\{|E_1\rangle, |E_2\rangle\}$ in Eq. (28) produces

$$\begin{pmatrix} |\mathcal{A}\rangle \\ |\mathcal{B}\rangle \end{pmatrix} = \frac{1}{\sqrt{1 + \delta^2}} \begin{pmatrix} 1 & e^{i\varphi_\alpha} \delta \\ e^{i\frac{\varphi_\alpha - \varphi_\beta}{2}} & e^{i\frac{\varphi_\alpha + \varphi_\beta}{2}} \delta \end{pmatrix} \begin{pmatrix} |E_1\rangle \\ |E_2\rangle \end{pmatrix}. \quad (29)$$

By inverting the matrix relation presented in Eq. (29), we derive a method to express $\{|E_1\rangle, |E_2\rangle\}$ in terms of $\{|\mathcal{A}\rangle, |\mathcal{B}\rangle\}$. Specifically, we achieve

$$\begin{pmatrix} |E_1\rangle \\ |E_2\rangle \end{pmatrix} = \frac{\sqrt{1 + \delta^2}}{e^{i\frac{\varphi_\alpha + \varphi_\beta}{2}} - e^{i\varphi_\alpha} e^{i\frac{\varphi_\alpha - \varphi_\beta}{2}}} \begin{pmatrix} e^{i\frac{\varphi_\alpha + \varphi_\beta}{2}} & -e^{i\varphi_\alpha} \\ -\frac{1}{\delta} e^{i\frac{\varphi_\alpha - \varphi_\beta}{2}} & \frac{1}{\delta} \end{pmatrix} \begin{pmatrix} |\mathcal{A}\rangle \\ |\mathcal{B}\rangle \end{pmatrix}. \quad (30)$$

Consequently, by utilizing Eqs. (27) and (30), we reach

$$\begin{pmatrix} |E_1\rangle \\ |E_2\rangle \end{pmatrix} = \frac{\sqrt{1 + \delta^2}}{e^{i\frac{\varphi_\alpha + \varphi_\beta}{2}} - e^{i\varphi_\alpha} e^{i\frac{\varphi_\alpha - \varphi_\beta}{2}}} \begin{pmatrix} e^{i\frac{\varphi_\alpha + \varphi_\beta}{2}} & -e^{i\varphi_\alpha} \\ -\frac{1}{\delta} e^{i\frac{\varphi_\alpha - \varphi_\beta}{2}} & \frac{1}{\delta} \end{pmatrix} \begin{pmatrix} \frac{\alpha_1^{-1}}{\sqrt{1 + \delta^2}} |A\rangle \\ \frac{\beta_1^{-1}}{\sqrt{1 + \delta^2}} e^{i\frac{\varphi_\alpha - \varphi_\beta}{2}} |B\rangle \end{pmatrix}. \quad (31)$$

Use of Eq. (30) leads to the expression for the quantum overlap $\langle \mathcal{A} | \mathcal{B} \rangle$,

$$\langle \mathcal{A} | \mathcal{B} \rangle = \cos\left(\frac{\varphi_\alpha - \varphi_\beta}{2}\right) + i \frac{1 - \delta^2}{1 + \delta^2} \sin\left(\frac{\varphi_\alpha - \varphi_\beta}{2}\right), \quad (32)$$

with $\langle \mathcal{B} | \mathcal{A} \rangle = \langle \mathcal{A} | \mathcal{B} \rangle^*$. From Eq. (32), the probability amplitude $|\langle \mathcal{A} | \mathcal{B} \rangle|^2$ reduces to

$$|\langle \mathcal{A} | \mathcal{B} \rangle|^2 = \frac{|\langle A | B \rangle|^2}{\langle A | A \rangle \langle B | B \rangle} = \frac{1 + 2\delta^2 \cos(\varphi_\alpha - \varphi_\beta) + \delta^4}{(1 + \delta^2)^2}. \quad (33)$$

As an additional remark, we emphasize that when $\delta = 1$, Eq. (33) simplifies to $|\langle \mathcal{A} | \mathcal{B} \rangle|^2 = \cos^2[(\varphi_\alpha - \varphi_\beta)/2]$. This equation represents what we anticipate in a time optimal context. Moreover, to confirm the second relation in Eq. (33), we observe that

$$\langle A | A \rangle = |\alpha_1|^2 + \delta^2 |\alpha_1|^2, \quad \langle B | B \rangle = |\beta_1|^2 + \delta^2 |\beta_1|^2, \quad \text{and} \quad |\langle A | B \rangle|^2 = \left| \alpha_1^* \beta_1 \left(1 + \delta^2 e^{-i(\varphi_\alpha - \varphi_\beta)} \right) \right|^2. \quad (34)$$

Therefore, after some algebra, we arrive at

$$\begin{aligned} \frac{|\langle A | B \rangle|^2}{\langle A | A \rangle \langle B | B \rangle} &= \frac{|\alpha_1^* \beta_1|^2 |1 + \delta^2 e^{-i(\varphi_\alpha - \varphi_\beta)}|^2}{(|\alpha_1|^2 + \delta^2 |\alpha_1|^2)(|\beta_1|^2 + \delta^2 |\beta_1|^2)} \\ &= \frac{|1 + \delta^2 e^{-i(\varphi_\alpha - \varphi_\beta)}|^2}{(1 + \delta^2)^2} \\ &= \frac{1 + 2\delta^2 \cos(\varphi_\alpha - \varphi_\beta) + \delta^4}{(1 + \delta^2)^2} \\ &= |\langle \mathcal{A} | \mathcal{B} \rangle|^2. \end{aligned} \quad (35)$$

It is worthwhile pointing out that Eq. (35) can be conveniently recast as

$$\frac{|\langle A | B \rangle|^2}{\langle A | A \rangle \langle B | B \rangle} = 1 - 4 \frac{\delta^2}{(1 + \delta^2)^2} \sin^2 \left(\frac{\varphi_\alpha - \varphi_\beta}{2} \right) = \cos^2 \left(\frac{\theta_{AB}}{2} \right), \quad (36)$$

with θ_{AB} being the geodesic distance between $|A\rangle$ and $|B\rangle$,

$$\theta_{AB} \stackrel{\text{def}}{=} 2 \arccos \left(\frac{|\langle A | B \rangle|}{\sqrt{\langle A | A \rangle} \sqrt{\langle B | B \rangle}} \right). \quad (37)$$

We are now ready to construct the time suboptimal Hamiltonian in an explicit manner. Observe that $H = E[-|E_1\rangle\langle E_1| + |E_2\rangle\langle E_2|]$. Using Eq. (30), we can express $|E_1\rangle\langle E_1|$ and $|E_2\rangle\langle E_2|$ in terms of $|\mathcal{A}\rangle\langle\mathcal{A}|$, $|\mathcal{A}\rangle\langle\mathcal{B}|$, $|\mathcal{B}\rangle\langle\mathcal{A}|$, and $|\mathcal{B}\rangle\langle\mathcal{B}|$. We have,

$$|E_1\rangle\langle E_1| = \frac{1 + \delta^2}{\left| e^{i\frac{\varphi_\alpha + \varphi_\beta}{2}} - e^{i\varphi_\alpha} e^{i\frac{\varphi_\alpha - \varphi_\beta}{2}} \right|^2} \left[|\mathcal{A}\rangle\langle\mathcal{A}| - e^{-i\varphi_\alpha} e^{i\frac{\varphi_\alpha + \varphi_\beta}{2}} |\mathcal{A}\rangle\langle\mathcal{B}| - e^{i\varphi_\alpha} e^{-i\frac{\varphi_\alpha + \varphi_\beta}{2}} |\mathcal{B}\rangle\langle\mathcal{A}| + |\mathcal{B}\rangle\langle\mathcal{B}| \right], \quad (38)$$

and,

$$|E_2\rangle\langle E_2| = \frac{1 + \delta^2}{\delta^2 \left| e^{i\frac{\varphi_\alpha + \varphi_\beta}{2}} - e^{i\varphi_\alpha} e^{i\frac{\varphi_\alpha - \varphi_\beta}{2}} \right|^2} \left[|\mathcal{A}\rangle\langle\mathcal{A}| - e^{i\frac{\varphi_\alpha - \varphi_\beta}{2}} |\mathcal{A}\rangle\langle\mathcal{B}| - e^{-i\frac{\varphi_\alpha - \varphi_\beta}{2}} |\mathcal{B}\rangle\langle\mathcal{A}| + |\mathcal{B}\rangle\langle\mathcal{B}| \right]. \quad (39)$$

After some algebra, inserting Eqs. (38) and (39) into $H = E[-|E_1\rangle\langle E_1| + |E_2\rangle\langle E_2|]$, we get

$$\begin{aligned} H &= E \frac{1 - \delta^2}{\delta^2} \frac{1 + \delta^2}{\left| e^{i\frac{\varphi_\alpha + \varphi_\beta}{2}} - e^{i\varphi_\alpha} e^{i\frac{\varphi_\alpha - \varphi_\beta}{2}} \right|^2} (|\mathcal{A}\rangle\langle\mathcal{A}| + |\mathcal{B}\rangle\langle\mathcal{B}|) + \\ &+ E \frac{1 + \delta^2}{\delta^2} \frac{1}{\left| e^{i\frac{\varphi_\alpha + \varphi_\beta}{2}} - e^{i\varphi_\alpha} e^{i\frac{\varphi_\alpha - \varphi_\beta}{2}} \right|^2} \left[\left(\delta^2 e^{-i\frac{\varphi_\alpha - \varphi_\beta}{2}} - e^{i\frac{\varphi_\alpha - \varphi_\beta}{2}} \right) |\mathcal{A}\rangle\langle\mathcal{B}| + \left(\delta^2 e^{i\frac{\varphi_\alpha - \varphi_\beta}{2}} - e^{-i\frac{\varphi_\alpha - \varphi_\beta}{2}} \right) |\mathcal{B}\rangle\langle\mathcal{A}| \right]. \end{aligned} \quad (40)$$

To further simplify the expression of H in Eq. (40) and express the time suboptimal Hamiltonian in terms of $|\mathcal{A}\rangle\langle\mathcal{A}|$, $|\mathcal{A}\rangle\langle\mathcal{B}|$, $|\mathcal{B}\rangle\langle\mathcal{A}|$, and $|\mathcal{B}\rangle\langle\mathcal{B}|$, we realize that

$$\left| e^{i\frac{\varphi_\alpha + \varphi_\beta}{2}} - e^{i\varphi_\alpha} e^{i\frac{\varphi_\alpha - \varphi_\beta}{2}} \right|^2 = 4 \sin^2 \left(\frac{\varphi_\alpha - \varphi_\beta}{2} \right). \quad (41)$$

From Eq. (27), we note that $|\mathcal{A}\rangle\langle\mathcal{A}|$ and $|\mathcal{B}\rangle\langle\mathcal{B}|$ can be recast as

$$|\mathcal{A}\rangle\langle\mathcal{A}| = \frac{|A\rangle\langle A|}{\langle A|A\rangle}, \text{ and } |\mathcal{B}\rangle\langle\mathcal{B}| = \frac{|B\rangle\langle B|}{\langle B|B\rangle}, \quad (42)$$

respectively. In addition, $|\mathcal{A}\rangle\langle\mathcal{B}|$ and $|\mathcal{B}\rangle\langle\mathcal{A}|$ become

$$|\mathcal{A}\rangle\langle\mathcal{B}| = \frac{1}{1+\delta^2} \frac{e^{-i\frac{\varphi_\alpha-\varphi_\beta}{2}}}{\alpha_1\beta_1^*} |A\rangle\langle B|, \text{ and } |\mathcal{B}\rangle\langle\mathcal{A}| = \frac{1}{1+\delta^2} \frac{e^{i\frac{\varphi_\alpha-\varphi_\beta}{2}}}{\alpha_1^*\beta_1} |B\rangle\langle A|, \quad (43)$$

respectively. To further simplify Eq. (43), we notice from Eq. (26) that

$$\alpha_1^*\beta_1 = \frac{e^{i\frac{\varphi_\alpha-\varphi_\beta}{2}}}{e^{i\frac{\varphi_\alpha-\varphi_\beta}{2}} + \delta^2 e^{-i\frac{\varphi_\alpha-\varphi_\beta}{2}}} \langle A|B\rangle, \quad (44)$$

with $\alpha_1\beta_1^* = (\alpha_1^*\beta_1)^*$. Then, making use of Eq. (44), the relations for $|\mathcal{A}\rangle\langle\mathcal{B}|$ and $|\mathcal{B}\rangle\langle\mathcal{A}|$ in Eq. (43) reduce to

$$|\mathcal{A}\rangle\langle\mathcal{B}| = \frac{e^{-i\frac{\varphi_\alpha-\varphi_\beta}{2}} + \delta^2 e^{i\frac{\varphi_\alpha-\varphi_\beta}{2}}}{1+\delta^2} \frac{|A\rangle\langle B|}{\langle B|A\rangle}, \text{ and } |\mathcal{B}\rangle\langle\mathcal{A}| = \frac{e^{i\frac{\varphi_\alpha-\varphi_\beta}{2}} + \delta^2 e^{-i\frac{\varphi_\alpha-\varphi_\beta}{2}}}{1+\delta^2} \frac{|B\rangle\langle A|}{\langle A|B\rangle}, \quad (45)$$

respectively. Finally, employing Eqs. (41), (42), and (45), the time suboptimal Hamiltonian in Eq. (40) can be recast as

$$\begin{aligned} H = E \frac{1-\delta^2}{\delta^2} \frac{1+\delta^2}{4\sin^2\left(\frac{\varphi_\alpha-\varphi_\beta}{2}\right)} & \left(\frac{|A\rangle\langle A|}{\langle A|A\rangle} + \frac{|B\rangle\langle B|}{\langle B|B\rangle} \right) + \\ & + E \frac{1+\delta^2}{\delta^2} \frac{1}{4\sin^2\left(\frac{\varphi_\alpha-\varphi_\beta}{2}\right)} \left[\begin{aligned} & \left(\delta^2 e^{-i\frac{\varphi_\alpha-\varphi_\beta}{2}} - e^{i\frac{\varphi_\alpha-\varphi_\beta}{2}} \right) \frac{e^{-i\frac{\varphi_\alpha-\varphi_\beta}{2}} + \delta^2 e^{i\frac{\varphi_\alpha-\varphi_\beta}{2}}}{1+\delta^2} \frac{|A\rangle\langle B|}{\langle B|A\rangle} \\ & + \left(\delta^2 e^{i\frac{\varphi_\alpha-\varphi_\beta}{2}} - e^{-i\frac{\varphi_\alpha-\varphi_\beta}{2}} \right) \frac{e^{i\frac{\varphi_\alpha-\varphi_\beta}{2}} + \delta^2 e^{-i\frac{\varphi_\alpha-\varphi_\beta}{2}}}{1+\delta^2} \frac{|B\rangle\langle A|}{\langle A|B\rangle} \end{aligned} \right]. \end{aligned} \quad (46)$$

Following additional algebraic manipulation and the application of Eq. (36), the Hamiltonian H as presented in Eq. (46) ultimately simplifies to

$$H_{\text{subopt}} = E \frac{\frac{1-\delta^2}{1+\delta^2}}{1-\cos^2\left(\frac{\theta_{AB}}{2}\right)} \left[\frac{|A\rangle\langle A|}{\langle A|A\rangle} + \frac{|B\rangle\langle B|}{\langle B|B\rangle} - \left(\frac{|A\rangle\langle B|}{\langle B|A\rangle} + \frac{|B\rangle\langle A|}{\langle A|B\rangle} \right) \right] + iE \cot\left(\frac{\varphi_\alpha-\varphi_\beta}{2}\right) \left(\frac{|B\rangle\langle A|}{\langle A|B\rangle} - \frac{|A\rangle\langle B|}{\langle B|A\rangle} \right), \quad (47)$$

where $H = H^\dagger$, $\text{tr}(H) = 0$, $\langle H \rangle = [(\delta^2 - 1) / (1 + \delta^2)] E$, $\Delta E = [2\delta / (1 + \delta^2)] E$ and, most importantly, $|\langle A|B\rangle|^2 / [\langle A|A\rangle\langle B|B\rangle] = 1 - [4\delta^2 / (1 + \delta^2)^2] \sin^2[(\varphi_\alpha - \varphi_\beta)/2] = \cos^2(\theta_{AB}/2)$. In summary, for the sake of thoroughness, we also highlight that when $\delta = 1$, H_{subopt} in Eq. (47) reduces to H_{opt} in Eq. (24).

Considering the Hamiltonians presented in Eqs. (24) and (47), we can examine the quantum evolution across a wide range of initial and final states, encompassing any level of entanglement. We will commence these investigations in the following section.

V. APPLICATIONS

We begin this section by examining two-qubit stationary evolutions that transition between separable and maximally entangled states. Our study encompasses four distinct types of Hamiltonian evolutions, utilizing both geometric and entanglement quantifiers. The four scenarios under consideration are: i) Time optimal evolutions between nonorthogonal quantum states; ii) Time suboptimal quantum evolutions between nonorthogonal states; iii) Time optimal evolutions between orthogonal quantum states; iv) Time suboptimal quantum evolutions between orthogonal states. In Table III, we present a summary of the characteristics pertaining to average entanglement, average entanglement speed, and the nonlocal properties of the unitary time propagators that will be examined in the subsequent subsections.

Evolution	Orthogonality	Average entanglement, \bar{C}	Average entanglement speed, \bar{v}_C	Nonlocal character, $\varepsilon_{EP}^{Yukalov}$
Optimal	No	Lower	Higher	Higher
Suboptimal	No	Higher	Lower	High
Optimal	Yes	Lower	Higher	High
Suboptimal	Yes	Higher	Lower	Higher

TABLE III: Summary of the characteristics of average entanglement \bar{C} , average entanglement speed \bar{v}_C , and the nonlocal properties of unitary time propagators quantified by $\varepsilon_{EP}^{Yukalov}$. We consider both time-optimal and time-suboptimal quantum evolutions between separable and maximally entangled states. Furthermore, both scenarios in which this pair of states is either nonorthogonal or orthogonal are examined.

A. Time optimal evolution between nonorthogonal states

In the initial application, we examine the time optimal evolution between a separable quantum state and a maximally entangled quantum state that are not orthogonal.

Specifically, we wish to evolve from $|A\rangle \stackrel{\text{def}}{=} |00\rangle$ to $|B\rangle \stackrel{\text{def}}{=} (|00\rangle + |11\rangle)/\sqrt{2}$ in a time-optimal manner, assuming $\Delta E \stackrel{\text{def}}{=} E/\sqrt{2}$. The choice of taking $\Delta E \stackrel{\text{def}}{=} E/\sqrt{2}$ is dictated by the fact that this choice allows for an energetically fair comparison with the time suboptimal evolution between the same nonorthogonal initial and final states $|A\rangle$ and $|B\rangle$, respectively, that we consider in the next example. Before finding the time optimal Hamiltonian, we can observe that in this scenario, the geodesic distance s_0 between $|A\rangle$ and $|B\rangle$ is $s_0 = 2 \arccos[|\langle A | B \rangle|] = \pi/2$. Therefore, assuming $\Delta E \stackrel{\text{def}}{=} E/\sqrt{2}$, the optimal time to arrive at $|B\rangle$ from $|A\rangle$ is given by $t_{\text{opt}} = [\hbar(\pi/4)]/(E/\sqrt{2}) = (\hbar\pi)/(2\sqrt{2}E)$. Having stated that, the matrix representation of the time optimal Hamiltonian in the canonical basis $\mathcal{B}_{\mathcal{H}_2^2} \stackrel{\text{def}}{=} \{|00\rangle, |01\rangle, |10\rangle, |11\rangle\}$ of \mathcal{H}_2^2 (i.e., the Hilbert space of two-qubit quantum states) is given by

$$H_{\text{opt}} = \frac{E}{\sqrt{2}} \begin{pmatrix} 0 & 0 & 0 & -i \\ 0 & 0 & 0 & 0 \\ 0 & 0 & 0 & 0 \\ i & 0 & 0 & 0 \end{pmatrix}. \quad (48)$$

For completeness, we note from Eq. (48) that $H_{\text{opt}} = H_{\text{opt}}^\dagger$, $\text{tr}(H_{\text{opt}}) = 0$, $\Delta E^2 = \langle H_{\text{opt}}^2 \rangle - \langle H_{\text{opt}} \rangle^2 = E^2/2$, $\eta_{\text{geo}} = 1$ (since $s = s_0$), $\eta_{\text{Uzdin}} = 1$, and $\kappa_{\text{AC}}^2 = 0$. After diagonalizing the matrix in Eq. (48), we find that the corresponding unitary time propagator $U_{\text{opt}}(t) = e^{-iH_{\text{opt}}t/\hbar}$ is given by

$$U_{\text{opt}}(t) = \begin{pmatrix} \cos(\frac{1}{\sqrt{2}}\frac{E}{\hbar}t) & 0 & 0 & -\sin(\frac{1}{\sqrt{2}}\frac{E}{\hbar}t) \\ 0 & 1 & 0 & 0 \\ 0 & 0 & 1 & 0 \\ \sin(\frac{1}{\sqrt{2}}\frac{E}{\hbar}t) & 0 & 0 & \cos(\frac{1}{\sqrt{2}}\frac{E}{\hbar}t) \end{pmatrix}, \quad (49)$$

with $U_{\text{opt}}(t)U_{\text{opt}}^\dagger(t) = U_{\text{opt}}^\dagger(t)U_{\text{opt}}(t) = \mathbf{1}_{4 \times 4}$, and $U_{\text{opt}}(t_{\text{opt}})|A\rangle = |B\rangle$. From an entanglement standpoint, we note that the entanglement $C(\gamma(t))$ of the path $\gamma(t) : t \mapsto |\psi(t)\rangle \stackrel{\text{def}}{=} U_{\text{opt}}(t)|A\rangle$ is given by $C(t) = C[|\psi(t)\rangle] = |\sin(\sqrt{2}\frac{E}{\hbar}t)| = \sin(\sqrt{2}\frac{E}{\hbar}t)$ for $0 \leq t \leq (\hbar\pi)/(2\sqrt{2}E)$. Moreover, the average path entanglement during the evolution defined as

$$\bar{C} = \frac{1}{t_{\text{opt}}} \int_0^{t_{\text{opt}}} C(t) dt, \quad (50)$$

is equal to $2/\pi \simeq 0.64$. Finally, to quantify the nonlocal and entangling character of the time propagator in Eq. (49), we calculate the entanglement production $\varepsilon_{EP}^{Yukalov}(t)$ in Eq. (6). After some algebra, we find

$$\varepsilon_{EP}^{Yukalov}(t) = \frac{1}{2} \log \left\{ \frac{4}{\left[1 + \cos(\frac{1}{\sqrt{2}}\frac{E}{\hbar}t) \right]^2} \right\}. \quad (51)$$

In the short-time limit, $\varepsilon_{\text{EP}}^{\text{Yukalov}}(t)$ exhibits a polynomially quadratic growth specified by the relation

$$\varepsilon_{\text{EP}}^{\text{Yukalov}}(t) = \frac{1}{8} \left(\frac{E}{\hbar} \right)^2 t^2 + \frac{1}{384} \left(\frac{E}{\hbar} \right)^4 t^4 + \mathcal{O}(t^6). \quad (52)$$

We observe, as expected, that $\varepsilon_{\text{EP}}^{\text{Yukalov}}(0) = 0$ in Eq. (51).

B. Time suboptimal evolution between nonorthogonal states

In the second application, we analyze the time suboptimal evolution that takes place between a separable quantum state and a maximally entangled quantum state that are not orthogonal.

We want to go from $|A\rangle \stackrel{\text{def}}{=} |00\rangle$ to $|B\rangle \stackrel{\text{def}}{=} (|00\rangle + |11\rangle)/\sqrt{2}$ in a suboptimal way with an Hamiltonian with energy variance $\Delta E^2 \stackrel{\text{def}}{=} (1/2)E^2$. Recall that the formal expression of a suboptimal Hamiltonian that connects $|A\rangle$ to $|B\rangle$ is given in Eq. (47), with $|\langle A|B\rangle|^2$ satisfying the condition in Eq. (36). Note that θ_{AB} in Eq. (36) is the geodesic distance s_0 which, in our case, equals $\pi/2$. Furthermore, since the variance ΔE^2 of H_{subopt} in Eq. (47) is $[4\delta^2/(1+\delta^2)^2]E^2$, we set in Eq. (36) $\delta \stackrel{\text{def}}{=} 1 + \sqrt{2}$ and $\varphi_\alpha - \varphi_\beta \stackrel{\text{def}}{=} \pi$. This way, with $\theta_{AB} = \pi/2$, $\delta \stackrel{\text{def}}{=} 1 + \sqrt{2}$, and $\varphi_\alpha - \varphi_\beta \stackrel{\text{def}}{=} \pi$, Eq. (36) is properly satisfied. Having said that, the matrix representation of the time suboptimal Hamiltonian in the canonical basis $\mathcal{B}_{\mathcal{H}_2^2} \stackrel{\text{def}}{=} \{|00\rangle, |01\rangle, |10\rangle, |11\rangle\}$ of \mathcal{H}_2^2 is given by

$$H_{\text{subopt}} = \frac{E}{\sqrt{2}} \begin{pmatrix} 1 & 0 & 0 & 1 \\ 0 & 0 & 0 & 0 \\ 0 & 0 & 0 & 0 \\ 1 & 0 & 0 & -1 \end{pmatrix}. \quad (53)$$

For thoroughness, we note from Eq. (53) that $H_{\text{subopt}} = H_{\text{subopt}}^\dagger$, $\text{tr}(H_{\text{subopt}}) = 0$, $\Delta E^2 = \langle H_{\text{subopt}}^2 \rangle - \langle H_{\text{subopt}} \rangle^2 = E^2/2$, $\eta_{\text{geo}} = 1/\sqrt{2} < 1$ (since $s = \sqrt{2}s_0$), $\eta_{\text{Uzdin}} = 1/\sqrt{2} < 1$, and the curvature coefficient in Eq. (19) does not depend on the energy E since it equals $\kappa_{\text{AC}}^2 = 4$. After diagonalizing the matrix in Eq. (53), we find that the corresponding unitary time propagator $U_{\text{subopt}}(t) = e^{-\frac{i}{\hbar}H_{\text{subopt}}t}$ is given by

$$U_{\text{subopt}}(t) = \begin{pmatrix} \cos(\frac{E}{\hbar}t) - \frac{i}{\sqrt{2}} \sin(\frac{E}{\hbar}t) & 0 & 0 & -\frac{i}{\sqrt{2}} \sin(\frac{E}{\hbar}t) \\ 0 & 1 & 0 & 0 \\ 0 & 0 & 1 & 0 \\ -\frac{i}{\sqrt{2}} \sin(\frac{E}{\hbar}t) & 0 & 0 & \cos(\frac{E}{\hbar}t) + \frac{i}{\sqrt{2}} \sin(\frac{E}{\hbar}t) \end{pmatrix}, \quad (54)$$

with $U_{\text{subopt}}(t)U_{\text{subopt}}^\dagger(t) = U_{\text{subopt}}^\dagger(t)U_{\text{subopt}}(t) = \mathbf{1}_{4 \times 4}$, and $U_{\text{subopt}}(t_*)|A\rangle = |B\rangle$ with $t_* = (\hbar\pi)/(2E) = \sqrt{2}t_{\text{opt}} > t_{\text{opt}}$. From an entanglement standpoint, we note that the entanglement $C(\gamma(t))$ of the path $\gamma(t) : t \mapsto |\psi(t)\rangle \stackrel{\text{def}}{=} U_{\text{subopt}}(t)|A\rangle$ is given by $C(t) = C[|\psi(t)\rangle] = 2\sqrt{\frac{3}{16} - \frac{1}{16}\cos^2(2\frac{E}{\hbar}t) - \frac{1}{8}\cos(2\frac{E}{\hbar}t)}$ for $0 \leq t \leq (\hbar\pi)/(2E)$. Moreover, the average path entanglement during the evolution, defined as $\bar{C} \stackrel{\text{def}}{=} (1/t_*) \int_0^{t_*} C(t) dt$, is equal to $[2\sqrt{2} + \cosh^{-1}(3)]/(2\pi) \simeq 0.73$ where “ \cosh^{-1} ” is the inverse hyperbolic cosine function. Finally, to quantify the nonlocal entangling character of the time propagator in Eq. (54), we calculate the entanglement production $\varepsilon_{\text{EP}}^{\text{Yukalov}}(t)$ in Eq. (6). After some algebra, we arrive at

$$\varepsilon_{\text{EP}}^{\text{Yukalov}}(t) = \frac{1}{2} \log \left\{ \frac{4 [2 \cos(\frac{E}{\hbar}t) + 2]^2}{[\cos^2(\frac{E}{\hbar}t) + 4 \cos(\frac{E}{\hbar}t) + 3]^2} \right\}. \quad (55)$$

In the short-time limit, $\varepsilon_{\text{EP}}^{\text{Yukalov}}(t)$ displays a polynomially quadratic growth defined by the relationship

$$\varepsilon_{\text{EP}}^{\text{Yukalov}}(t) = \frac{1}{8} \left(\frac{E}{\hbar} \right)^2 t^2 - \frac{1}{384} \left(\frac{E}{\hbar} \right)^4 t^4 + \mathcal{O}(t^6). \quad (56)$$

It is noted, as anticipated, that $\varepsilon_{\text{EP}}^{\text{Yukalov}}(0) = 0$ in Eq. (55).

C. Time optimal evolution between orthogonal states

In the third application, we investigate the time optimal evolution between a separable state and a maximally entangled state that are orthogonal.

Specifically, we wish to evolve from $|A\rangle \stackrel{\text{def}}{=} |00\rangle$ to $|B\rangle \stackrel{\text{def}}{=} (|01\rangle + |10\rangle)/\sqrt{2}$ in a time-optimal manner, assuming $\Delta E \stackrel{\text{def}}{=} \sqrt{5/2}E$. The choice of taking $\Delta E \stackrel{\text{def}}{=} \sqrt{5/2}E$ is dictated by the fact that this choice allows for an energetically fair comparison with the time suboptimal evolution between the same orthogonal initial and final states $|A\rangle$ and $|B\rangle$, respectively, that we consider in the next example. Before finding the time optimal Hamiltonian, we can observe that in this scenario, the geodesic distance s_0 between $|A\rangle$ and $|B\rangle$ is $s_0 = 2 \arccos[|\langle A | B \rangle|] = \pi$. Therefore, assuming $\Delta E \stackrel{\text{def}}{=} \sqrt{5/2}E$, the optimal time to arrive at $|B\rangle$ from $|A\rangle$ is given by $t_{\text{opt}} = [\hbar(\pi/2)]/(\sqrt{5/2}E) = (\hbar\pi)/(\sqrt{10}E)$. Having mentioned that, the matrix representation of the time optimal Hamiltonian $H_{\text{opt}} \stackrel{\text{def}}{=} i\Delta E [|B\rangle\langle A| - |A\rangle\langle B|]$ in the canonical basis $\mathcal{B}_{\mathcal{H}_2^2} \stackrel{\text{def}}{=} \{|00\rangle, |01\rangle, |10\rangle, |11\rangle\}$ of \mathcal{H}_2^2 is,

$$H_{\text{opt}} = E \frac{\sqrt{5}}{2} \begin{pmatrix} 0 & -i & -i & 0 \\ i & 0 & 0 & 0 \\ i & 0 & 0 & 0 \\ 0 & 0 & 0 & 0 \end{pmatrix}. \quad (57)$$

For exhaustiveness, we note from Eq. (57) that $H_{\text{opt}} = H_{\text{opt}}^\dagger$, $\text{tr}(H_{\text{opt}}) = 0$, $\Delta E^2 = \langle H_{\text{opt}}^2 \rangle - \langle H_{\text{opt}} \rangle^2 = (5/2)E^2$, $\eta_{\text{geo}} = 1$ (since $s = s_0 = \pi$), $\eta_{\text{Uzdin}} = 1$, and $\kappa_{\text{AC}}^2 = 0$. After diagonalizing the matrix in Eq. (57), we find that the corresponding unitary time propagator $U_{\text{opt}}(t) = e^{-iH_{\text{opt}}t}$ is given by

$$U_{\text{opt}}(t) = \begin{pmatrix} \cos(\frac{\sqrt{10}}{2} \frac{E}{\hbar} t) & -\frac{1}{\sqrt{2}} \sin(\frac{\sqrt{10}}{2} \frac{E}{\hbar} t) & -\frac{1}{\sqrt{2}} \sin(\frac{\sqrt{10}}{2} \frac{E}{\hbar} t) & 0 \\ \frac{1}{\sqrt{2}} \sin(\frac{\sqrt{10}}{2} \frac{E}{\hbar} t) & \cos^2(\frac{\sqrt{10}}{2} \frac{E}{\hbar} t) & -\sin^2(\frac{\sqrt{10}}{2} \frac{E}{\hbar} t) & 0 \\ \frac{1}{\sqrt{2}} \sin(\frac{\sqrt{10}}{2} \frac{E}{\hbar} t) & -\sin^2(\frac{\sqrt{10}}{2} \frac{E}{\hbar} t) & \cos^2(\frac{\sqrt{10}}{2} \frac{E}{\hbar} t) & 0 \\ 0 & 0 & 0 & 1 \end{pmatrix}, \quad (58)$$

with $U_{\text{opt}}(t)U_{\text{opt}}^\dagger(t) = U_{\text{opt}}^\dagger(t)U_{\text{opt}}(t) = \mathbf{1}_{4 \times 4}$, and $U_{\text{opt}}(t_{\text{opt}})|A\rangle = |B\rangle$ where $t_{\text{opt}} \stackrel{\text{def}}{=} (\hbar\pi)/(\sqrt{10}E)$. From an entanglement standpoint, we note that the entanglement $C(\gamma(t))$ of the path $\gamma(t) : t \mapsto |\psi(t)\rangle \stackrel{\text{def}}{=} U_{\text{opt}}(t)|A\rangle$ is given by $C(t) = C[|\psi(t)\rangle] = \sin^2(\frac{\sqrt{10}}{2} \frac{E}{\hbar} t)$ for $0 \leq t \leq t_{\text{opt}}$. Moreover, the average path entanglement during the evolution is $\bar{C} = 1/2$. Finally, to quantify the nonlocal entangling character of the time propagator in Eq. (58), we calculate the entanglement production $\varepsilon_{\text{EP}}^{\text{Yukalov}}(t)$ in Eq. (6). After some algebraic manipulations, we obtain

$$\varepsilon_{\text{EP}}^{\text{Yukalov}}(t) = \frac{1}{2} \log \left\{ \frac{4 \left[2 \cos(\frac{\sqrt{10}}{2} \frac{E}{\hbar} t) + 2 \right]^2}{\left[\frac{3}{2} \cos^2(\frac{\sqrt{10}}{2} \frac{E}{\hbar} t) + 3 \cos(\frac{\sqrt{10}}{2} \frac{E}{\hbar} t) + \frac{7}{2} \right]^2} \right\}. \quad (59)$$

In the short-time limit, $\varepsilon_{\text{EP}}^{\text{Yukalov}}(t)$ shows a polynomially quadratic growth characterized by the relation

$$\varepsilon_{\text{EP}}^{\text{Yukalov}}(t) = \frac{5}{16} \left(\frac{E}{\hbar} \right)^2 t^2 + \mathcal{O}(t^4). \quad (60)$$

It is observed, as foreseen, that $\varepsilon_{\text{EP}}^{\text{Yukalov}}(0) = 0$ in Eq. (59).

D. Time suboptimal evolution between orthogonal states

In the fourth application, we study the time suboptimal evolution that takes place between a separable quantum state and a maximally entangled quantum state, which are orthogonal.

To construct a suboptimal stationary Hamiltonian that connects two orthogonal states, it is necessary to exit the two-dimensional space spanned by initial and final states $|A\rangle$ and $|B\rangle$, respectively [69]. Therefore, we cannot use

our proposed suboptimal Hamiltonian construction in Section IV. Instead, we need to build an example by hand. We proceed as follows. Let us consider an Hamiltonian whose spectral decomposition is given by,

$$H \stackrel{\text{def}}{=} \sum_{i=1}^4 E_i |E_i\rangle \langle E_i|, \quad (61)$$

with $E_1 \stackrel{\text{def}}{=} -2E$, $E_2 \stackrel{\text{def}}{=} -E$, $E_3 \stackrel{\text{def}}{=} E$, $E_4 \stackrel{\text{def}}{=} 2E$, and $\langle E_i | E_j \rangle = \delta_{ij}$ for any $1 \leq i, j \leq 4$. We note that H in Eq. (61) is capable of evolving $|A\rangle \stackrel{\text{def}}{=} (1/2)[|E_1\rangle + |E_2\rangle + |E_3\rangle + |E_4\rangle]$ into $|B\rangle \stackrel{\text{def}}{=} (1/2)[|E_1\rangle - |E_2\rangle - |E_3\rangle + |E_4\rangle]$, with $\langle A | B \rangle = 0$ and $\Delta E = \sqrt{5/2}E$, in a time $t_* = (\pi\hbar)/E > t_{\text{opt}} = (\pi\hbar)/(\sqrt{10}E)$. Since we wish to have $|A\rangle \stackrel{\text{def}}{=} |00\rangle$ and $|B\rangle \stackrel{\text{def}}{=} (|01\rangle + |10\rangle)/\sqrt{2}$, we apply the Gram-Schmidt orthogonalization procedure to ultimately find a suitable matrix transformation that allows us to transition from the eigenvector basis $\mathcal{B}_{\text{diag}} \stackrel{\text{def}}{=} \{|E_1\rangle, |E_2\rangle, |E_3\rangle, |E_4\rangle\}$ to the canonical computational basis $\mathcal{B}_{\text{can}} \stackrel{\text{def}}{=} \{|00\rangle, |01\rangle, |10\rangle, |11\rangle\}$. Specifically, we arrive at the following two matricial relations

$$\begin{pmatrix} |00\rangle \\ |01\rangle \\ |10\rangle \\ |11\rangle \end{pmatrix} = \begin{pmatrix} \frac{1}{2} & \frac{1}{2} & \frac{1}{2} & \frac{1}{2} \\ \frac{1}{\sqrt{2}} & -\frac{1}{\sqrt{2}} & 0 & 0 \\ 0 & 0 & -\frac{1}{\sqrt{2}} & \frac{1}{\sqrt{2}} \\ \frac{1}{2} & \frac{1}{2} & -\frac{1}{2} & -\frac{1}{2} \end{pmatrix} \begin{pmatrix} |E_1\rangle \\ |E_2\rangle \\ |E_3\rangle \\ |E_4\rangle \end{pmatrix}, \text{ and } \begin{pmatrix} |E_1\rangle \\ |E_2\rangle \\ |E_3\rangle \\ |E_4\rangle \end{pmatrix} = \begin{pmatrix} \frac{1}{2} & \frac{1}{\sqrt{2}} & 0 & \frac{1}{2} \\ \frac{1}{2} & -\frac{1}{\sqrt{2}} & 0 & \frac{1}{2} \\ \frac{1}{2} & 0 & -\frac{1}{\sqrt{2}} & -\frac{1}{2} \\ \frac{1}{2} & 0 & \frac{1}{\sqrt{2}} & -\frac{1}{2} \end{pmatrix} \begin{pmatrix} |00\rangle \\ |01\rangle \\ |10\rangle \\ |11\rangle \end{pmatrix}. \quad (62)$$

From the second relation in Eq. (62), the eigenvector matrix M_H and its inverse M_H^\dagger are given by

$$M_H = \begin{pmatrix} \frac{1}{2} & \frac{1}{2} & \frac{1}{2} & \frac{1}{2} \\ \frac{1}{\sqrt{2}} & -\frac{1}{\sqrt{2}} & 0 & 0 \\ 0 & 0 & -\frac{1}{\sqrt{2}} & \frac{1}{\sqrt{2}} \\ \frac{1}{2} & \frac{1}{2} & -\frac{1}{2} & -\frac{1}{2} \end{pmatrix}, \quad (63)$$

and M_H^\dagger being the transpose of M_H in Eq. (63), respectively. Finally, we arrive at the matrix representation of our time suboptimal Hamiltonian in Eq. (61) with respect to the computational basis \mathcal{B}_{can} . We obtain,

$$[H_{\text{subopt}}]_{\mathcal{B}_{\text{can}}} = M_H [H_{\text{subopt}}]_{\mathcal{B}_{\text{diag}}} M_H^\dagger = H = E \begin{pmatrix} 0 & -\frac{1}{2\sqrt{2}} & \frac{1}{2\sqrt{2}} & -\frac{3}{2} \\ -\frac{1}{2\sqrt{2}} & -\frac{3}{2} & 0 & -\frac{1}{2\sqrt{2}} \\ \frac{1}{2\sqrt{2}} & 0 & \frac{3}{2} & -\frac{1}{2\sqrt{2}} \\ -\frac{3}{2} & -\frac{1}{2\sqrt{2}} & -\frac{1}{2\sqrt{2}} & 0 \end{pmatrix}. \quad (64)$$

In what follows, to avoid a cumbersome notation, we simply denote $[H_{\text{subopt}}]_{\mathcal{B}_{\text{can}}}$ in Eq. (64) as H_{subopt} . For the sake of completeness, we notice from Eq. (64) that $H_{\text{subopt}} = H_{\text{subopt}}^\dagger$, $\text{tr}(H_{\text{subopt}}) = 0$, $\Delta E^2 = \langle H_{\text{opt}}^2 \rangle - \langle H_{\text{opt}} \rangle^2 = (5/2)E^2$, $\eta_{\text{geo}} < 1$ (since $s = \sqrt{10}\pi > s_0 = \pi$), $\eta_{\text{Uzdin}} = (1/2)(\sqrt{5}/2) < 1$, and $\kappa_{\text{AC}}^2 = 9/25$. After diagonalizing the matrix in Eq. (64), we find that the corresponding unitary time propagator $U_{\text{subopt}}(t) = e^{-\frac{i}{\hbar}H_{\text{subopt}}t}$ reduces to

$$U_{\text{subopt}}(t) = \begin{pmatrix} \frac{\cos(\frac{E}{\hbar}t) + \cos(2\frac{E}{\hbar}t)}{2} & \frac{i}{\sqrt{2}}e^{i\frac{3}{2}\frac{E}{\hbar}t} \sin(\frac{1}{2}\frac{E}{\hbar}t) & -\frac{i}{\sqrt{2}}e^{-i\frac{3}{2}\frac{E}{\hbar}t} \sin(\frac{1}{2}\frac{E}{\hbar}t) & \frac{i}{2}\frac{\sin(\frac{E}{\hbar}t) + \sin(2\frac{E}{\hbar}t)}{2} \\ \frac{i}{\sqrt{2}}e^{i\frac{3}{2}\frac{E}{\hbar}t} \sin(\frac{1}{2}\frac{E}{\hbar}t) & e^{i\frac{3}{2}\frac{E}{\hbar}t} \cos(\frac{1}{2}\frac{E}{\hbar}t) & 0 & \frac{i}{\sqrt{2}}e^{i\frac{3}{2}\frac{E}{\hbar}t} \sin(\frac{1}{2}\frac{E}{\hbar}t) \\ -\frac{i}{\sqrt{2}}e^{-i\frac{3}{2}\frac{E}{\hbar}t} \sin(\frac{1}{2}\frac{E}{\hbar}t) & 0 & e^{-i\frac{3}{2}\frac{E}{\hbar}t} \cos(\frac{1}{2}\frac{E}{\hbar}t) & \frac{i}{\sqrt{2}}e^{-i\frac{3}{2}\frac{E}{\hbar}t} \sin(\frac{1}{2}\frac{E}{\hbar}t) \\ \frac{i}{2}\frac{\sin(\frac{E}{\hbar}t) + \sin(2\frac{E}{\hbar}t)}{2} & \frac{i}{\sqrt{2}}e^{i\frac{3}{2}\frac{E}{\hbar}t} \sin(\frac{1}{2}\frac{E}{\hbar}t) & \frac{i}{\sqrt{2}}e^{-i\frac{3}{2}\frac{E}{\hbar}t} \sin(\frac{1}{2}\frac{E}{\hbar}t) & \frac{\cos(\frac{E}{\hbar}t) + \cos(2\frac{E}{\hbar}t)}{2} \end{pmatrix}, \quad (65)$$

with $U_{\text{subopt}}(t)U_{\text{subopt}}^\dagger(t) = U_{\text{subopt}}^\dagger(t)U_{\text{subopt}}(t) = \mathbf{1}_{4 \times 4}$, and $U_{\text{subopt}}(t_*)|A\rangle = |B\rangle$ with $t_* = (\pi\hbar)/E > t_{\text{opt}} = (\pi\hbar)/(\sqrt{10}E)$. From an entanglement standpoint, we note that the entanglement $C(\gamma(t))$ of the path $\gamma(t) : t \mapsto |\psi(t)\rangle \stackrel{\text{def}}{=} U_{\text{subopt}}(t)|A\rangle$ is given by $C(t) = C[|\psi(t)\rangle] = 2\sqrt{\left[\frac{1}{8}\sin(2\frac{E}{\hbar}t) + \frac{1}{4}\sin(3\frac{E}{\hbar}t) + \frac{1}{8}\sin(4\frac{E}{\hbar}t)\right]^2 + \left[\frac{1}{4}\cos(\frac{E}{\hbar}t) - \frac{1}{4}\right]^2}$ for $0 \leq t \leq (\pi\hbar)/E$. Moreover, the average path entanglement during the evolution, defined as $\bar{C} \stackrel{\text{def}}{=} (1/t_*) \int_0^{t_*} C(t) dt$, is approximately equal to 0.71. Finally, to quantify the nonlocal entangling character of the time propagator in Eq.

(65), we calculate the entanglement production $\varepsilon_{\text{EP}}^{\text{Yukalov}}(t)$ in Eq. (6). Following a series of algebraic manipulations, we find

$$\varepsilon_{\text{EP}}^{\text{Yukalov}}(t) = \frac{1}{2} \log \left\{ \frac{\mathcal{N}(t)}{\mathcal{D}_1(t)\mathcal{D}_2(t)} \right\}, \quad (66)$$

where,

$$\begin{cases} \mathcal{N}(t) \stackrel{\text{def}}{=} 4 \left[2 \cos\left(\frac{E}{\hbar}t\right) + 2 \cos\left(2\frac{E}{\hbar}t\right) \right]^2, \\ \mathcal{D}_1(t) \stackrel{\text{def}}{=} \frac{3}{2} \cos\left(\frac{E}{\hbar}t\right) + \frac{1}{4} \cos\left(\frac{2E}{\hbar}t\right) + \frac{5}{2} \cos\left(\frac{3E}{\hbar}t\right) + \frac{1}{4} \cos\left(\frac{4E}{\hbar}t\right) + \frac{7}{2}, \\ \mathcal{D}_2(t) \stackrel{\text{def}}{=} \frac{3}{2} \cos\left(\frac{E}{\hbar}t\right) + \frac{5}{4} \cos\left(\frac{2E}{\hbar}t\right) + \frac{1}{2} \cos\left(\frac{3E}{\hbar}t\right) + \frac{5}{4} \cos\left(\frac{4E}{\hbar}t\right) + \frac{7}{2}. \end{cases} \quad (67)$$

In the short-time limit, $\varepsilon_{\text{EP}}^{\text{Yukalov}}(t)$ exhibits a polynomially quadratic growth specified by the relation

$$\varepsilon_{\text{EP}}^{\text{Yukalov}}(t) = \frac{5}{8} \left(\frac{E}{\hbar} \right)^2 t^2 + \mathcal{O}(t^4). \quad (68)$$

We observe, as expected, that $\varepsilon_{\text{EP}}^{\text{Yukalov}}(0) = 0$ in Eq. (66).

The temporal behavior of the entanglement associated with the evolution paths that define our four illustrative examples are presented in Fig. 1. When comparing time optimal (a) and time suboptimal (b) evolutions between nonorthogonal states $|00\rangle$ (separable) and $(|00\rangle + |11\rangle)/\sqrt{2}$ (maximally entangled), it is observed that the time optimal evolutions conclude in a shorter duration, without any energy waste, and without any bending of the trajectory. Additionally, from the perspective of entanglement analysis, optimal evolutions appear to occur with lower average path entanglement values, higher average entanglement speed $\bar{v}_C \stackrel{\text{def}}{=} 1/\Delta t_{|A\rangle \rightarrow |B\rangle}$, and, ultimately, a greater degree of nonlocal entangling character in their respective unitary time propagators. Similar findings are evident when contrasting time optimal (c) and time suboptimal (d) evolutions between orthogonal states $|00\rangle$ (separable) and $(|01\rangle + |10\rangle)/\sqrt{2}$ (maximally entangled). Nevertheless, several critical differences must be highlighted. Firstly, in the comparison of (c) and (d), only the time optimal evolution (c) occurs within a two-dimensional subspace of the complete four-dimensional Hilbert space. In contrast, the time suboptimal evolution (d) transpires within the entire four-dimensional space. Secondly, unlike the situation observed when comparing (a) and (b), in the analysis between (c) and (d), the nonlocal entangling character of the unitary time propagator associated with the time suboptimal Hamiltonian is more pronounced than that which characterizes the time optimal evolution. Lastly, when comparing the time suboptimal evolutions in (b) and (d), it is noted that while the time suboptimal evolution between orthogonal states (d) occurs along longer paths with smaller curvature and greater energy resource waste, the time suboptimal evolution between nonorthogonal states (b) takes place along shorter paths with higher curvature and reduced energy resource waste. We direct your attention to Table III for a summary of the insights we have gathered.

We have not employed Zanardi's entangling power $\varepsilon_{\text{EP}}^{\text{Zanardi}}(U)$ in Eq. (8) in our four illustrative examples discussed so far. The main reason for this absence is because of computational challenges and is due to the fact that none of the unitary time propagators in Eqs. (49), (54), (58), and (65) appears in the canonical form specified by Eq. (11). In the following section, we will endeavor to address this gap by presenting new and insightful applications.

VI. TIME OPTIMALITY, NONLOCALITY, AND ENTANGLING POWER

In this section, with the understanding that our primary goal is to acquire insight rather than to achieve generality, we examine the entanglement characteristics of three distinct unitary propagators that do not necessarily correspond to stationary Hamiltonians constructed in Section IV. Each of these evolutions is time-optimal and transitions from a separable state to a maximally entangled state. Additionally, the initial and final states are considered to be non-orthogonal. Notably, we demonstrate through explicit examples that: ii) $\varepsilon_{\text{EP}}^{\text{Zanardi}}(U_1) = \varepsilon_{\text{EP}}^{\text{Zanardi}}(U_2)$ does not necessarily indicate that U_1 and U_2 are part of the same equivalence class; ii) $\varepsilon_{\text{EP}}^{\text{Yukalov}}(U_1) = \varepsilon_{\text{EP}}^{\text{Yukalov}}(U_2)$ does not imply that U_1 and U_2 belong to the same equivalence class; iii) Time-optimal evolutions that are also energetically efficient (i.e., exhibiting high speed efficiency η_{Uzdin}) do not have to achieve Zanardi's entangling power values as elevated as those associated with inefficient time-optimal evolutions to attain the maximally entangled target state.

A. Example 1

We begin by examining the time optimal evolution between a separable quantum state and a maximally entangled quantum state that are not orthogonal. Specifically, we evolve from $|A\rangle \stackrel{\text{def}}{=} |01\rangle$ to $|B\rangle \stackrel{\text{def}}{=} \frac{1+i}{2}|01\rangle + \frac{1-i}{2}|10\rangle$ in a time-

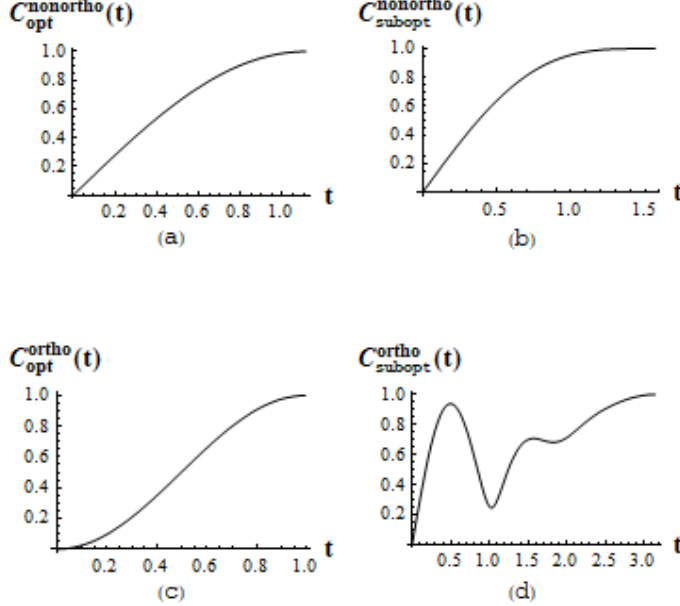


FIG. 1: In (a), there is a plot of the temporal behavior of the entanglement of the path that connects nonorthogonal initial (separable) and final (maximally entangled) states $|A\rangle \stackrel{\text{def}}{=} |00\rangle$ and $|B\rangle \stackrel{\text{def}}{=} [|00\rangle + |11\rangle] / \sqrt{2}$, respectively, when the evolution is time optimal. Entanglement is specified by the concurrence $C_{\text{opt}}^{\text{nonortho}}(t)$. Moreover, the unitary evolution occurs with energy dispersion $\Delta E = E / \sqrt{2}$ and $0 \leq t \leq (\pi\hbar) / (2\sqrt{2}E)$. In (b), there is a plot of the temporal behavior of the entanglement of the path that connects $|A\rangle \stackrel{\text{def}}{=} |00\rangle$ and $|B\rangle \stackrel{\text{def}}{=} [|00\rangle + |11\rangle] / \sqrt{2}$ when the evolution is time suboptimal. Entanglement is specified by the concurrence $C_{\text{subopt}}^{\text{nonortho}}(t)$. Moreover, the unitary evolution occurs with energy dispersion $\Delta E = E / \sqrt{2}$ and $0 \leq t \leq (\pi\hbar) / (2E)$. In (c), there is a plot of the temporal behavior of the entanglement of the path that connects orthogonal initial (separable) and final (maximally entangled) states $|A\rangle \stackrel{\text{def}}{=} |00\rangle$ and $|B\rangle \stackrel{\text{def}}{=} [|01\rangle + |10\rangle] / \sqrt{2}$, respectively, when the evolution is time optimal. Entanglement is specified by the concurrence $C_{\text{opt}}^{\text{ortho}}(t)$. Moreover, the unitary evolution occurs with energy dispersion $\Delta E = (\sqrt{5/2})E$ and $0 \leq t \leq (\pi\hbar) / (\sqrt{10}E)$. In (d), there is a plot of the temporal behavior of the entanglement of the path that connects $|A\rangle \stackrel{\text{def}}{=} |00\rangle$ and $|B\rangle \stackrel{\text{def}}{=} [|01\rangle + |10\rangle] / \sqrt{2}$ when the evolution is time suboptimal. Entanglement is specified by the concurrence $C_{\text{subopt}}^{\text{ortho}}(t)$. Moreover, the unitary evolution occurs with energy dispersion $\Delta E = (\sqrt{5/2})E$ and $0 \leq t \leq (\pi\hbar) / E$. In all plots, we set $E = 1$ and, finally, physical units are chosen using $\hbar = 1$.

optimal manner, with $\Delta E = E$ and $t_{\text{opt}} \stackrel{\text{def}}{=} (\hbar\pi) / (4E)$. This is accomplished by the non-local two-qubit Hamiltonian given by,

$$H \stackrel{\text{def}}{=} E(\sigma_x^{(1)} \otimes \sigma_x^{(2)}) + E(\sigma_z^{(1)} \otimes \sigma_z^{(2)}). \quad (69)$$

The matrix representation of the time optimal Hamiltonian in Eq. (69) with respect to the canonical basis $\mathcal{B}_{\mathcal{H}_2^2} \stackrel{\text{def}}{=} \{|00\rangle, |01\rangle, |10\rangle, |11\rangle\}$ of \mathcal{H}_2^2 is,

$$H = \begin{pmatrix} E & 0 & 0 & E \\ 0 & -E & E & 0 \\ 0 & E & -E & 0 \\ E & 0 & 0 & E \end{pmatrix}. \quad (70)$$

For completeness, we note from Eq. (70) that $H = H^\dagger$, $\text{tr}(H) = 0$, $\Delta E^2 = \langle H^2 \rangle - \langle H \rangle^2 = E^2$, $\eta_{\text{geo}} = 1$ (since $s = s_0 = \pi/2$), $\eta_{\text{Uzdin}} = 1/2 < 1$, and $\kappa_{\text{AC}}^2 = 0$. After diagonalizing the matrix in Eq. (70), we find that the

corresponding unitary time propagator $U(t) = e^{-\frac{i}{\hbar}Ht}$ is given by

$$U(t) = \begin{pmatrix} e^{-\frac{i}{\hbar}Et} \cos(\frac{E}{\hbar}t) & 0 & 0 & -ie^{-\frac{i}{\hbar}Et} \sin(\frac{E}{\hbar}t) \\ 0 & e^{\frac{i}{\hbar}Et} \cos(\frac{E}{\hbar}t) & -ie^{\frac{i}{\hbar}Et} \sin(\frac{E}{\hbar}t) & 0 \\ 0 & -ie^{\frac{i}{\hbar}Et} \sin(\frac{E}{\hbar}t) & e^{\frac{i}{\hbar}Et} \cos(\frac{E}{\hbar}t) & 0 \\ -ie^{-\frac{i}{\hbar}Et} \sin(\frac{E}{\hbar}t) & 0 & 0 & e^{-\frac{i}{\hbar}Et} \cos(\frac{E}{\hbar}t) \end{pmatrix}, \quad (71)$$

with $U(t)U^\dagger(t) = U^\dagger(t)U(t) = \mathbf{1}_{4 \times 4}$, and $U(t_{\text{opt}})|A\rangle = |B\rangle$. From an entanglement standpoint, we note that the entanglement $C(\gamma(t))$ of the path $\gamma(t) : t \mapsto |\psi(t)\rangle \stackrel{\text{def}}{=} U(t)|A\rangle$ is given by $C(t) = C(|\psi(t)\rangle) = |\sin(\frac{2E}{\hbar}t)| = \sin(\frac{2E}{\hbar}t)$ for $0 \leq t \leq (\hbar\pi)/(4E)$. Moreover, the average path entanglement equals $\bar{C} = 2/\pi \simeq 0.64$. To quantify the nonlocal entangling character of the time propagator in Eq. (71), we evaluate the entanglement production $\varepsilon_{\text{EP}}^{\text{Yukalov}}(t)$ in Eq. (6). After some algebra, we get

$$\varepsilon_{\text{EP}}^{\text{Yukalov}}(t) = \frac{1}{2} \log \left\{ \frac{4 [2 + 2 \cos(\frac{2E}{\hbar}t)]^2}{[8 \cos^4(\frac{E}{\hbar}t)]^2} \right\}. \quad (72)$$

In the short-time limit, $\varepsilon_{\text{EP}}^{\text{Yukalov}}(t)$ possesses a polynomially quadratic growth specified by the relation

$$\varepsilon_{\text{EP}}^{\text{Yukalov}}(t) = \left(\frac{E}{\hbar} \right)^2 t^2 + \frac{1}{6} \left(\frac{E}{\hbar} \right)^4 t^4 + \mathcal{O}(t^5). \quad (73)$$

We note, as expected, that $\varepsilon_{\text{EP}}^{\text{Yukalov}}(0) = 0$ in Eq. (72). Finally, inspecting the unitary evolution operator $U(t)$ in Eq. (71), we observe that its geometrical point is characterized by the vector \mathbf{c} given by

$$\mathbf{c} \stackrel{\text{def}}{=} (c_1, c_2, c_3) = \left(\frac{E}{\hbar}t, 0, \frac{E}{\hbar}t \right). \quad (74)$$

From Eq. (74), we also note that the entangling power $\varepsilon_{\text{EP}}^{\text{Zanardi}}(U)$ in Eq. (12) of this unitary operator U in Eq. (71) is equal to

$$\varepsilon_{\text{EP}}^{\text{Zanardi}}(t) = \frac{1}{18} \left[3 - \cos^2(\frac{4E}{\hbar}t) - 2 \cos(\frac{4E}{\hbar}t) \right]. \quad (75)$$

Interestingly, we observe from Eq. (75) that $\varepsilon_{\text{EP}}^{\text{Zanardi}}(0) = 0$ and $\varepsilon_{\text{EP}}^{\text{Zanardi}}(t_{\text{opt}}) = 2/9$, where $t_{\text{opt}} \stackrel{\text{def}}{=} (\hbar\pi)/(4E)$.

B. Example 2

Following the previous example, we continue by studying the optimal evolution between a separable quantum state and a maximally entangled quantum state that are not orthogonal. Specifically, we evolve from $|A\rangle \stackrel{\text{def}}{=} |01\rangle$ to $|B\rangle \stackrel{\text{def}}{=} \frac{1+i}{2}|01\rangle + \frac{1-i}{2}|10\rangle$ in a time-optimal manner, with $\Delta E = 2E$ and $t_{\text{opt}} \stackrel{\text{def}}{=} (\hbar\pi)/(8E)$. This is accomplished by the non-local two-qubit Hamiltonian defined as,

$$H \stackrel{\text{def}}{=} E(\sigma_x^{(1)} \otimes \sigma_x^{(2)}) + E(\sigma_y^{(1)} \otimes \sigma_y^{(2)}) + E(\sigma_z^{(1)} \otimes \sigma_z^{(2)}). \quad (76)$$

The matrix representation of H in the computational basis of the Hilbert space of two-qubit states is

$$H = \begin{pmatrix} E & 0 & 0 & 0 \\ 0 & -E & 2E & 0 \\ 0 & 2E & -E & 0 \\ 0 & 0 & 0 & E \end{pmatrix}. \quad (77)$$

For thoroughness, we note from Eq. (77) that $H = H^\dagger$, $\text{tr}(H) = 0$, $\Delta E^2 = \langle H^2 \rangle - \langle H \rangle^2 = 4E^2$, $\eta_{\text{geo}} = 1$ (since $s = s_0 = \pi/2$), $\eta_{\text{Uzdin}} = 2/3 < 1$, and $\kappa_{\text{AC}}^2 = 0$. After diagonalizing the matrix in Eq. (77), we find that the corresponding unitary time propagator $U(t) = e^{-\frac{i}{\hbar}Ht}$ is given by

$$U(t) = \begin{pmatrix} e^{-\frac{i}{\hbar}Et} & 0 & 0 & 0 \\ 0 & e^{\frac{i}{\hbar}Et} \cos(\frac{2E}{\hbar}t) & -ie^{\frac{i}{\hbar}Et} \sin(\frac{2E}{\hbar}t) & 0 \\ 0 & -ie^{\frac{i}{\hbar}Et} \sin(\frac{2E}{\hbar}t) & e^{\frac{i}{\hbar}Et} \cos(\frac{2E}{\hbar}t) & 0 \\ 0 & 0 & 0 & e^{-\frac{i}{\hbar}Et} \end{pmatrix}, \quad (78)$$

with $U(t)U^\dagger(t) = U^\dagger(t)U(t) = \mathbf{1}_{4 \times 4}$, and $U(t_{\text{opt}})|A\rangle = |B\rangle$. From an entanglement standpoint, we note that the entanglement $C(\gamma(t))$ of the path $\gamma(t) : t \mapsto |\psi(t)\rangle \stackrel{\text{def}}{=} U(t)|A\rangle$ is given by $C(t) = C[|\psi(t)\rangle] = |\sin(\frac{4E}{\hbar}t)| = \sin(\frac{4E}{\hbar}t)$ for $0 \leq t \leq (\hbar\pi)/(8E)$. Moreover, the average path entanglement equals $\bar{C} = 2/\pi \simeq 0.64$. To quantify the nonlocal entangling character of the time propagator in Eq. (78), we calculate the entanglement production $\varepsilon_{\text{EP}}^{\text{Yukalov}}(t)$ in Eq. (6). After some algebraic manipulations, we arrive at

$$\varepsilon_{\text{EP}}^{\text{Yukalov}}(t) = \frac{1}{2} \log \left\{ \frac{4[10 + 6\cos(\frac{4E}{\hbar}t)]}{[3\cos(\frac{4E}{\hbar}t) + 5]^2} \right\} \quad (79)$$

In the short-time limit, $\varepsilon_{\text{EP}}^{\text{Yukalov}}(t)$ exhibits a polynomially quadratic growth specified by the relation

$$\varepsilon_{\text{EP}}^{\text{Yukalov}}(t) = \frac{3}{2} \left(\frac{E}{\hbar} \right)^2 t^2 + \frac{1}{4} \left(\frac{E}{\hbar} \right)^4 t^4 + \mathcal{O}(t^6). \quad (80)$$

We observe, as expected, that $\varepsilon_{\text{EP}}^{\text{Yukalov}}(0) = 0$ in Eq. (79). Finally, from $U(t)$ in Eq. (78), we observe that the geometrical point is specified by the vector \mathbf{c} given by

$$\mathbf{c} \stackrel{\text{def}}{=} (c_1, c_2, c_3) = \left(\frac{E}{\hbar}t, \frac{E}{\hbar}t, \frac{E}{\hbar}t \right). \quad (81)$$

From Eq. (81), we also note that the entangling power $\varepsilon_{\text{EP}}^{\text{Zanardi}}(U)$ in Eq. (12) of this unitary operator U in Eq. (78) is equal to

$$\varepsilon_{\text{EP}}^{\text{Zanardi}}(t) = \frac{1}{6} \sin^2\left(\frac{4E}{\hbar}t\right). \quad (82)$$

We note from Eq. (82) that $\varepsilon_{\text{EP}}^{\text{Zanardi}}(0) = 0$ and $\varepsilon_{\text{EP}}^{\text{Zanardi}}(t_{\text{opt}}) = 1/6$, where $t_{\text{opt}} \stackrel{\text{def}}{=} (\hbar\pi)/(8E)$.

C. Example 3

In this last example, we wish to evolve from $|A\rangle \stackrel{\text{def}}{=} |01\rangle$ to $|B\rangle \stackrel{\text{def}}{=} \frac{1+i}{2}|01\rangle + \frac{1-i}{2}|10\rangle$ in a time-optimal manner, with $\Delta E = 2E$ and $t_{\text{opt}} \stackrel{\text{def}}{=} (\hbar\pi)/(8E)$. This was accomplished in the second example. However, we want to construct an alternative time-independent Hamiltonian here. We proceed as follows. Consider the Hamiltonian H given by Eq. (24) with $\Delta E \stackrel{\text{def}}{=} 2E$, $|A\rangle \stackrel{\text{def}}{=} |01\rangle$, and $|B\rangle \stackrel{\text{def}}{=} \frac{1+i}{2}|01\rangle + \frac{1-i}{2}|10\rangle$. After some algebra, the matrix representation of this H in the computational basis of the Hilbert space of two-qubit states becomes

$$H = 2E \begin{pmatrix} 0 & 0 & 0 & 0 \\ 0 & 0 & 1 & 0 \\ 0 & 1 & 0 & 0 \\ 0 & 0 & 0 & 0 \end{pmatrix}. \quad (83)$$

For the sake of completeness, we point out from Eq. (83) that $H = H^\dagger$, $\text{tr}(H) = 0$, $\Delta E^2 = \langle H^2 \rangle - \langle H \rangle^2 = 4E^2$, $\eta_{\text{geo}} = 1$ (since $s = s_0 = \pi/2$), $\eta_{\text{Uzdin}} = 1$, and $\kappa_{\text{AC}}^2 = 0$. After diagonalizing the matrix in Eq. (77), we find that the corresponding unitary time propagator $U(t) = e^{-\frac{i}{\hbar}Ht}$ becomes

$$U(t) = \begin{pmatrix} 1 & 0 & 0 & 0 \\ 0 & \cos\left(\frac{2E}{\hbar}t\right) & -i\sin\left(\frac{2E}{\hbar}t\right) & 0 \\ 0 & -i\sin\left(\frac{2E}{\hbar}t\right) & \cos\left(\frac{2E}{\hbar}t\right) & 0 \\ 0 & 0 & 0 & 1 \end{pmatrix}, \quad (84)$$

with $U(t)U^\dagger(t) = U^\dagger(t)U(t) = \mathbf{1}_{4 \times 4}$, and $U(t_{\text{opt}})|A\rangle = |B\rangle$. From an entanglement standpoint, we note that the entanglement $C(\gamma(t))$ of the path $\gamma(t) : t \mapsto |\psi(t)\rangle \stackrel{\text{def}}{=} U(t)|A\rangle$ is given by $C(t) = C[|\psi(t)\rangle] = |\sin(\frac{4E}{\hbar}t)| = \sin(\frac{4E}{\hbar}t)$ for $0 \leq t \leq (\hbar\pi)/(8E)$. Moreover, the average path entanglement equals $\bar{C} = 2/\pi \simeq 0.64$. To characterize the nonlocal

entangling character of the time propagator in Eq. (84), we calculate the entanglement production $\varepsilon_{\text{EP}}^{\text{Yukalov}}(t)$ in Eq. (6). After some algebra, we find

$$\varepsilon_{\text{EP}}^{\text{Yukalov}}(t) = \frac{1}{2} \log \left\{ \frac{4 \left[2 + 2 \cos \left(\frac{2E}{\hbar} t \right) \right]^2}{\left[8 \cos^4 \left(\frac{E}{\hbar} t \right) \right]^2} \right\} \quad (85)$$

In the short-time limit, $\varepsilon_{\text{EP}}^{\text{Yukalov}}(t)$ shows a polynomially quadratic growth specified by the relation

$$\varepsilon_{\text{EP}}^{\text{Yukalov}}(t) = \left(\frac{E}{\hbar} \right)^2 t^2 + \frac{1}{6} \left(\frac{E}{\hbar} \right)^4 t^4 + \mathcal{O}(t^5). \quad (86)$$

We observe, as expected, that $\varepsilon_{\text{EP}}^{\text{Yukalov}}(0) = 0$ in Eq. (72). Finally, from $U(t)$ in Eq. (78), we observe that the geometrical point is specified by the vector \mathbf{c} given by

$$\mathbf{c} \stackrel{\text{def}}{=} (c_1, c_2, c_3) = \left(\frac{E}{\hbar} t, \frac{E}{\hbar} t, 0 \right). \quad (87)$$

From Eq. (87), we also note that the entangling power of this unitary operator is equal to

$$\varepsilon_{\text{EP}}^{\text{Zanardi}}(t) = \frac{1}{18} \left[3 - \cos^2 \left(\frac{4E}{\hbar} t \right) - 2 \cos \left(\frac{4E}{\hbar} t \right) \right]. \quad (88)$$

Interestingly, we observe from Eq. (88) that $\varepsilon_{\text{EP}}^{\text{Zanardi}}(0) = 0$, $\varepsilon_{\text{EP}}^{\text{Zanardi}}(t_{\text{opt}}) = 1/6$, and $\varepsilon_{\text{EP}}^{\text{Zanardi}}(2t_{\text{opt}}) = 2/9$, where $t_{\text{opt}} \stackrel{\text{def}}{=} (\hbar\pi)/(8E)$.

It is evident that all unitary operators within the same equivalence class exhibit an equal level of entangling power. However, the reverse is not necessarily the case. For instance, when we compare Example 1 with Example 3, we observe that the unitary time propagators represented in Eqs. (71) and (84) do not belong to the same equivalence class, as the parameter \mathbf{c} in Eq. (74) differs from that in Eq. (87). Nevertheless, these operators correspond to quantum evolutions that yield identical entanglement productions $\varepsilon_{\text{EP}}^{\text{Yukalov}}$ (with Eqs. (72) and (85) being identical) and entangling powers $\varepsilon_{\text{EP}}^{\text{Zanardi}}$ (with Eqs. (75) and (88) being the same). Additionally, when we compare Example 2 to Example 3, we discover that time-optimal evolutions that are also energetically efficient (as seen in Eq. (84), Example 3) do not necessarily need to achieve entangling power values of $\varepsilon_{\text{EP}}^{\text{Zanardi}}$ that are as high as those linked to energetically inefficient time-optimal evolutions (as indicated in Eq. (78), Example 2) in order to reach maximally entangled target states. A comparative analysis of the temporal behaviors of path entanglement, Yukalov's entanglement production, and Zanardi's entangling power for the quantum evolutions studied in Examples 2 and 3 is illustrated in Fig. 2.

We are now prepared to present our summary of results and final observations.

VII. FINAL REMARKS

In this paper, we studied relevant geometric properties of entanglement that emerge from time-independent nonlocal Hamiltonian evolutions transitioning from separable to maximally entangled two-qubit quantum states. From a geometric viewpoint, each evolution is defined by geodesic efficiency (Eq. (13)), speed efficiency (Eq. (15)), and curvature coefficient (Eq. (19)). On the other hand, from the perspective of entanglement, these evolutions are assessed using various metrics, including concurrence (Eq. (1)), entanglement power (Eq. (6)), and entangling capability (Eq. (8)).

When analyzing time optimal (Eq. (49)) and time suboptimal (Eq. (54)) evolutions between separable and maximally entangled *nonorthogonal* states (first scenario), we noted that the time optimal evolutions conclude in a shorter time frame, without any energy loss, and without any deviation from the geodesic trajectory (i.e., zero curvature). Furthermore, from the standpoint of entanglement analysis, optimal evolutions seem to occur with lower average path entanglement values, higher average entanglement speed, and ultimately, a greater degree of nonlocal entangling character in their respective unitary time propagators. Similar observations are apparent when comparing time optimal (Eq. (58)) and time suboptimal (Eq. (65)) evolutions between separable and maximally entangled *orthogonal* states (second scenario). However, several significant differences must be emphasized. Firstly, in this second scenario, only the time optimal evolution takes place within a two-dimensional subspace of the complete four-dimensional Hilbert space. In contrast, the time suboptimal evolution occurs throughout the entire four-dimensional space. Secondly, unlike the first scenario, in the second scenario, the nonlocal entangling character of the unitary time propagator

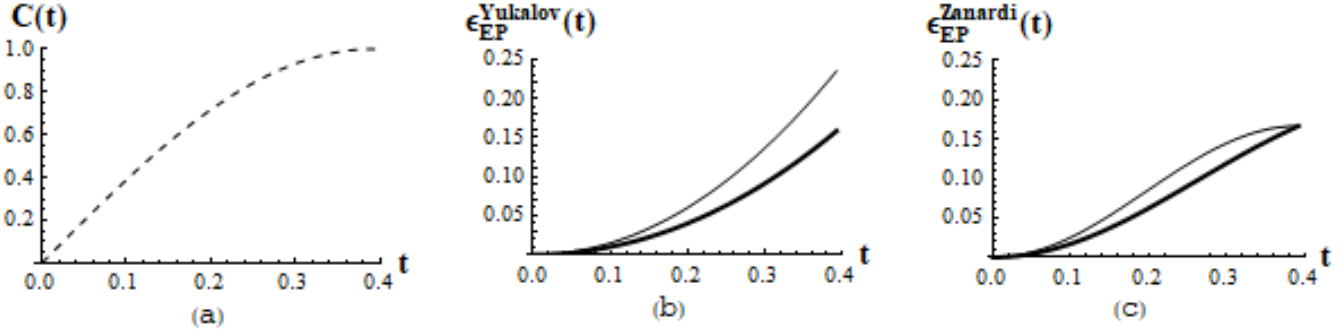


FIG. 2: Entanglement-based comparative analysis of two distinct optimal time evolutions (Example 2 and Example 3) from an initial (separable) state to a final (maximally entangled) state $|A\rangle \stackrel{\text{def}}{=} |01\rangle$ and $|B\rangle \stackrel{\text{def}}{=} \frac{1+i}{2}|01\rangle + \frac{1-i}{2}|10\rangle$, respectively, with $|\langle A | B \rangle| \neq 0$. In (a), there is a plot of the temporal behavior of the entanglement of the paths that connect $|A\rangle$ and $|B\rangle$. State entanglement is specified by the concurrence $C(t)$ which exhibits an identical time behavior in both cases. Both unitary time evolutions occur with energy dispersion $\Delta E = 2E$ and $0 \leq t \leq (\pi\hbar)/(8E)$. In (b), the nonlocal character of the unitary time propagators is captured by Yukalov's entanglement production $\epsilon_{\text{EP}}^{\text{Yukalov}}(t)$ versus time t for Example 2 (thin solid line) and Example 3 (thick solid line). In (c), the entanglement capability of the unitary time propagators is characterized by Zanardi's entanglement power $\epsilon_{\text{EP}}^{\text{Zanardi}}(t)$ versus time t for Example 2 (thin solid line) and Example 3 (thick solid line). Observe that $[\epsilon_{\text{EP}}^{\text{Zanardi}}((\pi\hbar)/(8E))]_{\text{Example-2}} = [\epsilon_{\text{EP}}^{\text{Zanardi}}((\pi\hbar)/(8E))]_{\text{Example-3}} = 1/6$. In all plots, we set $E = 1$ and, finally, physical units are chosen using $\hbar = 1$.

associated with the time suboptimal Hamiltonian is more pronounced than that which characterizes the time optimal evolution. Finally, when analyzing the time suboptimal evolutions in both the first and second scenarios, it is observed that the time suboptimal evolution between orthogonal states occurs along longer trajectories characterized by lower curvature and increased energy resource expenditure, whereas the time suboptimal evolution between nonorthogonal states transpires along shorter trajectories with higher curvature and diminished energy resource expenditure. These findings concerning the first part of our study are presented in Section V and are partially summarized in Table III and Fig. 1.

It is clear that all unitary operators within the same equivalence class demonstrate an equivalent degree of entangling power. However, the converse is not necessarily true. In fact, we provided specific examples where the unitary time propagators (Eqs. (71) and (84)) do not belong to the same equivalence class, yet these operators are associated with quantum evolutions that produce identical levels of entanglement production and entangling power. Furthermore, we found that time-optimal evolutions that are also energetically efficient (Eq. (84)) do not have to achieve entangling power values as high as those associated with energetically inefficient (Eq. (78)) time-optimal evolutions to attain maximally entangled target states within the same timeframe. The results of this second part of our study are detailed in Section VI and are partially encapsulated in Fig. 2. In the interest of thoroughness, we wish to emphasize that the formulation of the time suboptimal Hamiltonian presented in Eq. (47) constitutes another important finding disclosed in this paper, which builds upon our earlier results documented in Ref. [33].

Although we thoroughly examined points [i] (Eq. (47)) and [ii] (Eq. (65)) as discussed in the Introduction, our findings yielded insights rather than a comprehensive understanding regarding points [iii]-[vi] (Sections V and VI). Our work is subject to three limitations: (a) it is confined to stationary Hamiltonian evolutions, (b) it concentrates on specific initial and final states, and (c) it assesses the entangling power solely for unitary time propagators that are inherently in their canonical form. We intend to address some of these limitations in our future research endeavors. Nevertheless, despite these constraints, we believe that the results presented here are sufficiently significant to facilitate further geometric explorations of quantum evolutions in higher-dimensional systems (beyond two-qubit quantum states), where efficiency, curvature, and entanglement are crucial for the quantum-mechanical manipulation of these physical systems [70–73].

ACKNOWLEDGMENTS

C.C. is grateful to the Griffiss Institute (Rome-NY) and to the United States Air Force Research Laboratory (AFRL) Visiting Faculty Research Program (VFRP) for providing support for this work. J.S. acknowledges support from the AFRL. The authors wish to convey their appreciation for the insightful discussions conducted with P. M. Alsing. Any opinions, findings and conclusions or recommendations expressed in this material are those of the authors and do not necessarily reflect the views of the AFRL.

- [1] A. Peres and W. K. Wootters, *Optical detection of quantum information*, Phys. Rev. Lett. **66**, 1119 (1991).
- [2] C. H. Bennett, D. P. DiVincenzo, Ch. A. Fuchs, T. Mor, E. Rains, P. W. Shor, J. A. Smolin, and W. K. Wootters, *Quantum nonlocality without entanglement*, Phys. Rev. **A59**, 1070 (1999).
- [3] S. Halder, M. Banik, S. Agrawal, and S. Bandyopadhyay, *Strong quantum nonlocality without entanglement*, Phys. Rev. Lett. **122**, 040403 (2019).
- [4] S. Bhattacharya, S. Saha, T. Guha, and M. Banik, *Nonlocality without entanglement: Quantum theory and beyond*, Phys. Rev. Research **2**, 012068(R) (2020).
- [5] J. S. Bell, *On the Einstein Podolsky Rosen paradox*, Physics **1**, 195 (1964).
- [6] J. F. Clauser, M. A. Horne, A. Shimony, and R. A. Holt, *Proposed experiment to test local hidden variable theories*, Phys. Rev. Lett. **23**, 880 (1969).
- [7] A. Aspect, P. Grangier, and G. Roger, *Experimental realization of Einstein-Podolsky-Rosen-Bohm Gedankenexperiment: A new violation of Bell's inequalities*, Phys. Rev. Lett. **49**, 91 (1982).
- [8] C. Cafaro, Ch. Corda, P. Cairns, and A. Bingolbali, *Violation of Bell's inequality in the Clauser-Horne-Shimony Holt form with entangled quantum states revisited*, Int. J. Theor. Phys. **63**, 112 (2024).
- [9] D. Collins, N. Linden, and S. Popescu, *Nonlocal content of quantum operations*, Phys. Rev. **A64**, 032302 (2001).
- [10] W. Dur, G. Vidal, J. I. Cirac, N. Linden, and S. Popescu, *Entanglement capabilities of nonlocal Hamiltonians*, Phys. Rev. Lett. **87**, 137901 (2001).
- [11] V. Giovannetti, S. Lloyd, and L. Maccone, *The role of entanglement in dynamical evolution*, Europhys. Lett. **62**, 615 (2003).
- [12] V. Giovannetti, S. Lloyd, and L. Maccone, *Quantum limits to dynamical evolution*, Phys. Rev. **A67**, 052109 (2003).
- [13] V. Giovannetti, S. Lloyd, and L. Maccone, *The speed limit of quantum unitary evolution*, J. Opt. B: Quantum Semiclass. Opt. **6**, S807 (2004).
- [14] J. Batle, M. Casas, A. Plastino, and A. R. Plastino, *Connection between entanglement and the speed of quantum evolution*, Phys. Rev. **A72**, 032337 (2005).
- [15] J. Batle, M. Casas, A. Plastino, and A. R. Plastino, *Erratum: Connection between entanglement and the speed of quantum evolution*, Phys. Rev. **A73**, 049904(E) (2006).
- [16] A. Borras, M. Casas, A. R. Plastino, and A. Plastino, *Entanglement and the lower bounds on the speed of quantum evolution*, Phys. Rev. **A74**, 022326 (2006).
- [17] S. Curilef, C. Zander, and A. R. Plastino, *Two particles in a double well: Illustrating the connection between entanglement and the speed of quantum evolution*, Eur. J. Phys. **27**, 1193 (2006).
- [18] C. Zander, A. R. Plastino, A. Plastino, and M. Casas, *Entanglement and the speed of evolution of multi-partite quantum systems*, J. Phys. A: Math. Theor. **40**, 2861 (2007).
- [19] S. Curilef, C. Zander, and A. R. Plastino, *Speed of quantum evolution of entangled two qubit states: Local vs. global evolution*, J. Phys.: Conf. Ser. **134**, 012003 (2008).
- [20] H. F. Chau, *Comment on “Connection between entanglement and the speed of quantum evolution”*, Phys. Rev. **A82**, 056301 (2010).
- [21] J. Kupferman and B. Reznik, *Entanglement and the speed of evolution in mixed states*, Phys. Rev. **A78**, 042305 (2008).
- [22] F. Frowis, *Kind of entanglement that speeds up quantum evolution*, Phys. Rev. **A85**, 052127 (2012).
- [23] L. Rudnicki, *Quantum speed limit and geometric measure of entanglement*, Phys. Rev. **A104**, 032417 (2021).
- [24] D. Shrimali, S. Bhowmick, V. Pandey, and A. K. Pati, *Capacity of entanglement for a nonlocal Hamiltonian*, Phys. Rev. **A106**, 042419 (2022).
- [25] V. Pandey, D. Shrimali, B. Mohan, S. Das, and A. K. Pati, *Speed limits on correlations in bipartite quantum systems*, Phys. Rev. **A107**, 052419 (2023).
- [26] V. Pandey, S. Bhowmick, B. Mohan, Sohail, and U. Sen, *Fundamental speed limits on entanglement dynamics of bipartite quantum systems*, Phys. Rev. **A110**, 052420 (2024).
- [27] P. Deb, *Geometry of quantum state space and quantum correlations*, Quantum Inf. Process. **15**, 1629 (2016).
- [28] P. Bej and P. Deb, *Geometry of quantum state space and entanglement*, Quantum Inf. Process. **18**, 72 (2019).
- [29] S. Luo, *Wigner-Yanase skew information and uncertainty relations*, Phys. Rev. Lett. **91**, 180403 (2003).
- [30] A. M. Frydryszak, M. Gieysztor, and A. Kuzmak, *Probing the geometry of two-qubit state space by evolution*, Quantum Inf. Process. **18**, 84 (2019).
- [31] Z. H. Saleem et al., *Quantum Fisher information and the curvature of entanglement*, arXiv:quant-ph/2504.13729 (2025).
- [32] J. Anandan and Y. Aharonov, *Geometry of quantum evolution*, Phys. Rev. Lett. **65**, 1697 (1990).

-
- [33] C. Cafaro and P. M. Alsing, *Qubit geodesics on the Bloch sphere from optimal-speed Hamiltonian evolutions*, *Class. Quantum Grav.* **40**, 115005 (2023).
- [34] L. Rossetti, C. Cafaro, and N. Bahreyni, *Constructions of optimal-speed quantum evolutions: A comparative study*, *Physica Scripta* **99**, 095121 (2024).
- [35] R. Uzdin, U. Günther, S. Rahav, and N. Moiseyev, *Time-dependent Hamiltonians with 100% evolution speed efficiency*, *J. Phys. A: Math. Theor.* **45**, 415304 (2012).
- [36] L. Rossetti, C. Cafaro, and P. M. Alsing, *Deviations from geodesic evolutions and energy waste on the Bloch sphere*, *Phys. Rev. A* **111**, 022441 (2025).
- [37] P. M. Alsing and C. Cafaro, *From the classical Frenet–Serret apparatus to the curvature and torsion of quantum-mechanical evolutions. Part I. Stationary Hamiltonians*, *Int. J. Geom. Methods Mod. Phys.* **21**, 2450152 (2024).
- [38] P. M. Alsing and C. Cafaro, *From the classical Frenet–Serret apparatus to the curvature and torsion of quantum-mechanical evolutions. Part II. Nonstationary Hamiltonians*, *Int. J. Geom. Methods Mod. Phys.* **21**, 2450151 (2024).
- [39] C. Cafaro, L. Rossetti, and P. M. Alsing, *Curvature of quantum evolutions for qubits in time-dependent magnetic fields*, *Phys. Rev. A* **111**, 012408 (2025).
- [40] W. K. Wootters, *Entanglement of formation of an arbitrary state of two qubits*, *Phys. Rev. Lett.* **80**, 2245 (1998).
- [41] A. Shimony, *Degree of entanglement*, *Annals of the New York Academy of Sciences* **755**, 675 (1995).
- [42] V. I. Yukalov and E. P. Yukalova, *Evolutional entanglement production*, *Phys. Rev. A* **92**, 052121 (2015).
- [43] P. Zanardi, C. Zalka, and L. Faoro, *Entangling power of quantum evolutions*, *Phys. Rev. A* **62**, 030301(R) (2000).
- [44] S. A. Hill and W. K. Wootters, *Entanglement of a pair of quantum bits*, *Phys. Rev. Lett.* **78**, 5022 (1997).
- [45] W. K. Wootters, *Entanglement of formation and concurrence*, *Quantum Information and Computation* **1**, 27 (2001).
- [46] C. P. Williams, *Explorations in Quantum Computing*, Springer-Verlag London (2011).
- [47] S. L. Braunstein and C. M. Caves, *Statistical distance and the geometry of quantum states*, *Phys. Rev. Lett.* **72**, 3439 (1994).
- [48] T.-C. Wei and P. M. Goldbart, *Geometric measure of entanglement and applications to bipartite and multipartite quantum states*, *Phys. Rev. A* **68**, 042307 (2003).
- [49] V. I. Yukalov, *Entanglement measure for composite systems*, *Phys. Rev. Lett.* **90**, 167905 (2003).
- [50] V. I. Yukalov, *Quantifying entanglement production of quantum operators*, *Phys. Rev. A* **68**, 022109 (2003).
- [51] V. I. Yukalov and E. P. Yukalova, *Entanglement production by evolution operator*, *Journal of Physics: Conf. Series* **826**, 012021 (2017).
- [52] A. J. Coleman and V. I. Yukalov, *Reduced Density Matrices*, Springer-Verlag (2000).
- [53] V. I. Yukalov, *Matrix order indices in statistical mechanics*, *Physica A* **310**, 413 (2002).
- [54] C. Witte and M. Trucks, *A new entanglement measure induced by the Hilbert-Schmidt norm*, *Phys. Lett. A* **257**, 14 (1999).
- [55] J. Magne Leinaas, J. Myrheim, and E. Ovrum, *Geometrical aspects of entanglement*, *Phys. Rev. A* **74**, 012313 (2006).
- [56] V. I. Yukalov, *Order indices and entanglement production in quantum systems*, *Entropy* **22**, 565 (2020).
- [57] P. Pandya, O. Sakarya, and M. Wiesniak, *Hilbert-Schmidt distance and entanglement witnessing*, *Phys. Rev. A* **102**, 012409 (2020).
- [58] J. Siewert, *On orthogonal bases in the Hilbert-Schmidt space of matrices*, *J. Phys. Commun.* **6**, 055014 (2022).
- [59] P. Zanardi, *Entanglement of quantum evolutions*, *Phys. Rev. A* **63**, 040304(R) (2001).
- [60] X. Wang and P. Zanardi, *Quantum entanglement of unitary operators on bi-partite systems*, *Phys. Rev. A* **66**, 044303 (2002).
- [61] A. T. Rezakhani, *Characterization of two-qubit perfect entanglers*, *Phys. Rev. A* **70**, 052313 (2004).
- [62] S. Balakrishnan and R. Sankaranarayanan, *Entangling power and local invariants of two-qubit gates*, *Phys. Rev. A* **82**, 034301 (2010).
- [63] C. Cafaro and S. Mancini, *A geometric algebra perspective on quantum computational gates and universality in quantum computing*, *Advances in Applied Clifford Algebras* **21**, 493 (2011).
- [64] C. Cafaro, S. Ray, and P. M. Alsing, *Geometric aspects of analog quantum search evolutions*, *Phys. Rev. A* **102**, 052607 (2020).
- [65] P. M. Alsing and C. Cafaro, *Upper limit on the acceleration of a quantum evolution in projective Hilbert space*, *Int. J. Geom. Methods Mod. Phys.* **21**, 2440009 (2024).
- [66] J. Samuel and R. Bhandari, *General setting for Berry's phase*, *Phys. Rev. Lett.* **60**, 2339 (1988).
- [67] P. M. Alsing, C. Cafaro, O. Luongo, C. Lupo, S. Mancini, and H. Quevedo, *Comparing metrics for mixed quantum states: Sjöqvist and Bures*, *Phys. Rev. A* **107**, 052411 (2023).
- [68] A. Mostafazadeh, *Hamiltonians generating optimal-speed evolutions*, *Phys. Rev. A* **79**, 014101 (2009).
- [69] D. C. Brody, *Elementary derivation for passage times*, *J. Phys.: Math. Gen.* **36**, 5587 (2003).
- [70] B. Hetenyi and P. Levay, *Fluctuations, uncertainty relations, and the geometry of quantum state manifolds*, *Phys. Rev. A* **108**, 032218 (2023).
- [71] C. Chryssomalakos et al., *Curves in quantum state space, geometric phases, and the brachistophase*, *J. Phys. A: Math. Theor.* **56**, 285301 (2023).
- [72] C. Chryssomalakos et al., *Speed axcess and total acceleration: A kinematical approach to entanglement*, *Phys. Scr.* **99**, 125116 (2024).
- [73] D. D'Alessandro, *Introduction to Quantum Control and Dynamics*, Chapman and Hall/CRC (2021).